CoA Note No. 101

THE COLLEGE OF AERONAUTICS

CRANFIELD

ON SURFACE PRESSURE FLUCTUATIONS IN TURBULENT BOUNDARY LAYERS

by

G. M. LILLEY and T. H. HODGSON

NOTE NO. 101

April, 1960

THE COLLEGE OF AERONAUTICS

CRANFIELD

On Surface Pressure Fluctuations in Turbulent Boundary Layers*

- by -

G. M. Lilley, M.Sc., D.I.C., and
T. H. Hodgson, B.Sc., D.L.C., D.C.Ae.

SUMMARY

Existing work on the pressure fluctuations in turbulent shear flows is briefly reviewed with special reference to the problem of wall turbulence.

An approximate theory for the pressure fluctuations on the wall under both a turbulent boundary layer and a wall jet is given and indicates in the latter case an intensity many times that corresponding to the flow over a flat plate at zero pressure gradient, as typified by measurements on the wall of a wind tunnel. Experiments on a wall jet confirm these predictions and details of the few preliminary data are presented.

The results from the wall jet suggest that the intensity of the pressure fluctuations in the regions of adverse pressure gradient, on wings and bodies approaching and beyond separation will be higher than in regions of zero pressure gradient.

Appendices are included which deal with the necessary extensions to the analysis to fit the velocity correlation functions as measured by Grant (1958), the effects of time delay and eddy convection.

---

* To be read at the AGARD symposium on Boundary Layer Research in London, April 1960. This work was performed under the Ministry of Aviation Contract No. 7/GEN/1664/PR3.

CONTENTS

		Page
	Summary	
	List of Symbols	
1.	Introduction	1
2.	Theory of the pressure fluctuations in a shear flow	2
3.	Pressure fluctuations due to the 'inner region' shear flow	12
4.	Pressure fluctuations due to the 'outer mixing region' shear flow	15
5.	The spectrum and space pressure correlation for zero time delay	16
6.	The wall jet - Theory of the mean flow	17
7.	Apparatus	19
8.	Preliminary Results and Discussion	21
9.	Future Work	22
10.	Conclusions	22
11.	References	23
	Appendix A - The pressure equation for the wall jet	25
	Appendix B - The evaluation of an integral	27
	Appendix C - The structure of the large eddies near the wall in a turbulent boundary layer	30
	Appendix D - On space-time correlations of the fluctuating velocity and pressure	37
	Appendix E - The evaluation of the pressure spectrum	42
	Figures	

LIST OF SYMBOLS

A	amplitude
a_1, a_2, a_3	amplitude of big eddy velocity covariances
$c_f \equiv \tau_w / \frac{1}{2}\rho\ u_m^2$	skin friction coefficient
D	jet diameter
f	longitudinal velocity correlation coefficient (isotropic turbulence)
G, G_o, G_i, G_+, G_-	Green's functions
K	Von Karman constant
$\ell, \ell_p, \ell_1, \ell_2$	scales of turbulence
P	pressure covariance
$\bar{P}$	pressure spectrum function
p	pressure
$\sqrt{\overline{p^2}}$	r.m.s. value of pressure fluctuations
q	source density
R, ϕ, Z	cylindrical polar co-ordinates
R_{ij}, R_{ZZ}	velocity covariance
$\bar{R}_{ij}, \bar{R}_{ZZ}$	velocity correlation coefficient
$\underset{\sim}{r} \equiv (r_1, r_2, r_3)$	
$\underset{\sim}{r}' \equiv (r_1', r_2', r_3', r_4')$	
S	area
t	time
(u_R, u_ϕ, u_Z)	velocity components
$\bar{u}_R, \bar{u}_\phi, \bar{u}_Z$	mean velocity components
$\underset{\sim}{u} \equiv (u_1, u_2, u_3)$	velocity
u_m	maximum velocity at a given R
u_∞	free stream velocity

List of Symbols (Continued)

u_τ	shear velocity
$\bar{u}_c$	convection speed
V	volume
$\underset{\sim}{x}$, $\underset{\sim}{y}$, $\underset{\sim}{z}$	co-ordinates
$Z_{\frac{1}{2}}$, Z_m	distance to mid and maximum velocity in the outer region respectively
$\alpha = \bar{u}_Z^2 / u_\tau^2$, and	anisotropy factor
α_1, α_2, α_3	reciprocals of typical turbulence scales
δ	Dirac function, boundary layer thickness
δ_1	displacement thickness
κ	wave number
μ	viscosity
ν	kinematic viscosity; reciprocal of eddy lifetime
$\underset{\sim}{\xi}$	$\underset{\sim}{x}' - \underset{\sim}{x}$
ρ	density
τ	time delay
τ, τ_{RZ}	mean shear
τ_m	optimum time delay
τ_w	wall shear stress
ω	circular frequency
$(\ )_b$	denotes big eddy contribution
$(\ )_s$	denotes small eddy contribution
$^m(\ )$	denotes 'in moving frame of reference'
$^f(\ )$	denotes 'in fixed frame of reference'
$'$	denotes fluctuating quantities (but generally omitted)

1. Introduction

A knowledge of the intensity and spectra of the pressure fluctuations in turbulent shear flows is required in a wide range of aeronautical and hydrodynamic problems today. Such problems range from aerodynamic noise generated by turbulent motion, the vibrations of the aircraft skin at high speeds and the transmission of noise to the cabin and cockpit, to mention just a few.

Although work in this area was pioneered by Heisenberg (1948), Obukhoff (1949), Batchelor (1951) and Kraichnan (1956a and b), it is only relatively recently that experimental data has been obtained to check the theoretical data, and to set the pattern for investigations into more complicated situations, where the theory at the best would be very tentative. The work of Kraichnan is of particular interest for it deals with pressure fluctuations in the presence of a mean shear, and also in the case of wall turbulence, and therefore has direct application to the problem of wall pressure fluctuations under a turbulent boundary layer. (The earlier work of Heisenberg, Obukhoff and Batchelor considered only the case of isotropic turbulence). Kraichnan showed that on a wall $\sqrt{\overline{p^2}}/\frac{1}{2}\rho u_m^2 \sim \beta c_f$, where β is a factor between 2 and 12. Experimental results obtained by Willmarth (1959) and Harrison (1958) confirmed Kraichnan's predictions and gave values of β between 2.5 and 5.0.

The effect of Mach number on wall pressure fluctuations, although of obvious current importance, will not be considered here. Indeed the flow will be assumed incompressible throughout and the problem of boundary layer noise, that is the noise radiated away from the surface, will hardly be touched upon. Our attention will mainly be restricted to problems of wall turbulence, including the wall jet, and will not consider in the same detail pressure fluctuations in free turbulence. A review paper covering the items omitted by the authors, would naturally be of considerable topical interest, but it was felt that, bearing in mind the considerable efforts present in this area today and the present state of flux of knowledge in the subject, a greater need was for a fundamental appreciation of relatively simple flow models. The surface over which the fluid flows will be treated as rigid, and no account will be given of the response of the structure to pressure fluctuations.

The theory of the pressure fluctuations in wall turbulence, including the wall jet, will be treated on similar lines to the method used by Kraichnan 1956b). In this method the intensity of the pressure fluctuations can be obtained once the two-point velocity correlations, mean velocity gradient, and the turbulence intensity and scale are known. Experimental results obtained by Townsend (1956) Laufer (1955) and Grant (1958) will be used to find $\overline{p^2}$ on the wall. For the wall jet the mean flow theory due to Glauert (1956) will be adopted, together with results in the mean flow by Bakke (1957) and Bradshaw and Love (1959). The prediction in this case for $\overline{p^2}$ will be compared with those obtained from measurements.

Finally in order to avoid confusion in the theoretical treatment and the discussion of results, the authors stress that they are dealing with the problem of pressure fluctuations in a pseudo-incompressible turbulent shear flow. They prefer, and agree that it is one of personal preference and not one agreed by convention, to refer to boundary layer noise as the sound energy radiated away from the turbulent flow. This latter problem considered by Curle (1955), Phillips (1956) and Doak (1960) though connected has obvious differences from the present treatment.

2. Theory of the pressure fluctuations in a shear flow

In most instances where the pressure fluctuations are significant the fluctuations in the fluid density are significant also. The present problem is no exception. However since we will be more concerned with the pressure fluctuations inside the turbulent shear flow, which in our problem will be an essentially 'low speed flow', than the noise radiated from it, we may safely assume that the flow is incompressible. The equations of continuity and motion are therefore respectively

$$\frac{\partial u_i}{\partial x_i} = 0 \qquad (1)$$

$$\frac{\partial \rho u_i}{\partial t} + \frac{\partial}{\partial x_j} \rho u_i u_j = - \frac{\partial p}{\partial x_i} + \mu \nabla^2 u_i \qquad (2)$$

If we take the time derivative of (1) from the divergence of (2) we obtain the following equation for the pressure distribution

$$\nabla^2 p = - \rho \frac{\partial^2 u_i u_j}{\partial x_i \partial x_j} \qquad (3)$$

This shows that, whereas in inviscid steady flow the pressure at a point follows immediately from the dynamic pressure at the same point, the pressure at a point in a turbulent flow, since it obeys an equation of the Poisson type, is governed by fluctuations in velocity throughout the entire flow and not just at the field point.

In the problem of the wall jet the mean pressure is approximately constant everywhere, and the mean velocity field is radially symmetric so that in terms of cylindrical polar co-ordinates (R, ϕ, Z), the velocity components are given by $\bar{u}_R$ (R, Z), $\bar{u}_\phi = 0$ and $\bar{u}_Z$ (R, Z).

Since equation (3) above can be written alternatively in vector notation as

$$\nabla^2 p = -\rho \nabla . (\underset{\sim}{u} . \nabla) \underset{\sim}{u} \tag{3a}$$

we find on expanding the right hand side and making the usual boundary layer assumption that (see Appendix A)

$$\nabla^2 p \doteq -\rho \left(\frac{\partial u'_R}{\partial R} \cdot \frac{\partial \bar{u}_R}{\partial R} + 2 \frac{\partial u'_Z}{\partial R} \cdot \frac{\partial \bar{u}_R}{\partial Z} \right) \tag{4}$$

where (u'_R, u'_ϕ, u'_Z) denote the fluctuating components of velocity and $(\bar{u}_R, \bar{u}_\phi, \bar{u}_Z)$ the mean values.

But $\frac{\partial \bar{u}_R}{\partial R} << \frac{\partial \bar{u}_R}{\partial Z}$ so that finally we have

$$\nabla^2 p = -2\rho \frac{\partial u'_Z}{\partial R} \frac{\partial \bar{u}_R}{\partial Z} \tag{5}$$

$$= -2\rho \tau_{RZ} \frac{\partial u'_Z}{\partial R} \tag{5a}$$

where $\tau_{RZ}(R,Z) \equiv \frac{\partial \bar{u}_R}{\partial Z}$ is the local mean shear.

This result is similar to that found by Kraichnan (1956b) for the boundary layer flow over a flat plate with a mean velocity in the (x_1) direction varying with (x_2) only, the direction normal to the plate.

In order to simplify the notation, in what follows, we will drop the subscripts on τ and the primes on u_Z. Thus p and $\underset{\sim}{u}$ will now refer to the fluctuating pressure and velocity respectively, and τ is the mean shear. Therefore we can write equation (5a) in the equivalent form

$$\nabla^2 p = -2\rho\tau \frac{\partial u_Z}{\partial R} = -q(\underset{\sim}{x}, t) \tag{6}$$

where $q(\underset{\sim}{x}, t)$ is the source density. We are here assuming that the pressure fluctuations due to the amplifying effect of the mean shear on the turbulence, are greater than that due to the interaction of the turbulence on itself. Kraichnan (1956b) justifies the use of this assumption by showing that, approximately, the former will give rise to a root mean square value of pressure about 10 db higher over that due to the latter.

The solution of (6) can be found by finding an appropriate Green function, $G(\underset{\sim}{x}, \underset{\sim}{x}')$, which satisfies the boundary conditions. Since the Green function satisfies

$$\nabla^2 G(\underset{\sim}{x}, \underset{\sim}{x}') = - \delta(\underset{\sim}{x} - \underset{\sim}{x}') \qquad (7)$$

where $\delta(y)$ is the Dirac delta function, the appropriate solution of (6) is

$$p(\underset{\sim}{x}, t) = \int_V q(\underset{\sim}{y}, t)\, G(\underset{\sim}{x}, \underset{\sim}{y})\, d\underset{\sim}{y} + \int_S \left(G \frac{\partial p}{\partial n}(\underset{\sim}{y}, t) - p(\underset{\sim}{y}, t) \frac{\partial G}{\partial n} \right) . \, dS(\underset{\sim}{y}) \qquad \ldots\ldots \quad (8)$$

where V is the total volume occupied by the flow and S is the total area of the plane over which the fluid flows, provided at some initial time p and $\frac{\partial p}{\partial t}$ vanish. Here n is the normal to S, measured to the surface from the volume.

If we write G_- the Green function which vanishes on the plane S, G_+ the Green function given by

$$\frac{\partial G_+}{\partial n} = 0$$

on the plane S, and G_o the Green function for unbounded space, we have

$$\left.\begin{aligned} G_- &= G_o - G_i \\ G_+ &= G_o + G_i \end{aligned}\right\} \qquad (9)$$

where G_i is the Green function for the image point in the boundary. Hence we can find three equivalent solutions of (6), which depend on the particular choice of Green function. Thus

$$p(\underset{\sim}{x}, t) = \int_V q\, G_+ \, dV + \int_S G_+ \frac{\partial p}{\partial n} \, dS \qquad (10a)$$

$$= \int_V q\, G_- \, dV - \int_S p \frac{\partial G_-}{\partial n} \, dS \qquad (10b)$$

$$= \int_V q\, G_o \, dV + \int_S \left(G_o \frac{\partial p}{\partial n} - p \frac{\partial G_o}{\partial n} \right) dS \qquad (10c)$$

But on S we have

$$\left.\begin{aligned} G_o &= G_i \\ \frac{\partial G_o}{\partial n} &= - \frac{\partial G_i}{\partial n} \end{aligned}\right\} \qquad (11)$$

and so (10) can be written alternatively

$$p(\underset{\sim}{x}, t) = \int_V q\,(G_o + G_i)\, dV + 2 \int_S G_o \frac{\partial p}{\partial n} \, dS \qquad (12a)$$

$$= \int_V q\,(G_o - G_i)\, dV - 2 \int_S p \frac{\partial G_o}{\partial n} \, dS \qquad (12b)$$

$$= \int_V q\, G_o \, dV + \int_S (G_o \frac{\partial p}{\partial n} - p \frac{\partial G_o}{\partial n}) \, dS \qquad (12c)$$

The particular choice of one of these equations must depend on what is known about p and $\frac{\partial p}{\partial n}$ on the plane S. Clearly if $\frac{\partial p}{\partial n} = 0$ on S we would choose (12a).

Now the equation of motion in the Z-direction at Z = 0, where $u_R = u_\phi = u_Z = 0$, is

$$0 = -\frac{\partial p}{\partial Z} + \mu \frac{\partial^2 u_Z}{\partial Z^2} \tag{13}$$

for the fluctuating quantities and

$$0 = \mu \frac{\partial^2 \bar{u}_Z}{\partial Z^2} \tag{14}$$

for the mean flow.

But from the equation of continuity

$$\frac{\partial \bar{u}_Z}{\partial Z}, \quad \frac{\partial u_Z}{\partial Z} = 0 \quad \text{at} \quad Z = 0 \tag{15}$$

and therefore near the wall

$$\bar{u}_Z^2 = \frac{Z^4}{4\mu^2} \overline{\left(\frac{\partial p}{\partial Z}\right)^2} + \ldots\ldots \tag{16}$$

From the measured distribution of $\overline{u_Z^2}$ near the wall of a flat plate, channel or pipe Townsend (1956) finds that, (in our notation),

$$\overline{\left(\frac{\partial p}{\partial Z}\right)^2} \approx 3.4 \times 10^{-4} \frac{\tau_w^3}{\rho \nu^2} \tag{17}$$

where $\tau_w(R)$ is the wall mean shear stress given by

$$\tau_w \equiv \left(\mu \frac{\partial \bar{u}_R}{\partial Z}\right)_{Z=0} \tag{18}$$

Although $\overline{\left(\frac{\partial p}{\partial Z}\right)^2}$, as shown by (17) is a very small quantity we are not immediately justified in putting $\left(\frac{\partial p}{\partial Z}\right)_{Z=0} = 0$ in (12a).

However, if ℓ_1 is a typical length over which the velocity is correlated and ℓ_2 a similar length with respect to pressure, we see that the contributions to $\overline{p^2}$, from the volume and surface integrals in (12a), are in the ratio

$$100 \quad \ell_1^2 \; : \; \ell_2^2 \; .$$

Now if anything ℓ_2 is less than ℓ_1 and is certainly not large compared with ℓ_1, and so we see that the surface integral in (12a) can be neglected in agreement with Kraichnan's approximation (1956b). Thus we note that for this problem the solutions (12b) and (12c) are of less value than the first.

We therefore write approximately

$$p(\underset{\sim}{x}, t) = \frac{\rho}{2\pi} \int_V (|\underset{\sim}{x} - \underset{\sim}{y}|^{-1} + |\underset{\sim}{x} - \underset{\sim}{y}^*|^{-1}) \tau(\underset{\sim}{y}) \frac{\partial u_Z}{\partial R}(\underset{\sim}{y}) \, dV \quad \ldots\ldots (19)$$

on inserting $q(\underset{\sim}{x}, t)$ from (6) into (12a), and noting that

$$G_o + G_i = \frac{1}{4\pi} \left(\frac{1}{|\underset{\sim}{x} - \underset{\sim}{y}|} + \frac{1}{|\underset{\sim}{x} - \underset{\sim}{y}^*|} \right) \qquad (20)$$

where $\underset{\sim}{y}^* = \underset{\sim}{y}(R, \phi, -Z)$, and the volume of integration is over the half-space $Z > 0$.

On the surface of the plane $\underset{\sim}{x} \equiv (R, \phi, 0)$ so that

$$p(\underset{\sim}{x}, t)_{Z=0} = \frac{\rho}{\pi} \int_{Z>0} \frac{\tau(\underset{\sim}{y}) \frac{\partial u_Z}{\partial R}(\underset{\sim}{y})}{|\underset{\sim}{x} - \underset{\sim}{y}|} \, d\underset{\sim}{y} \qquad (21)$$

and the pressure covariance, for zero time delay between the pressures at $\underset{\sim}{x}$ and $\underset{\sim}{x}'$ respectively, is

$$\mathbb{P}(\underset{\sim}{x}; \underset{\sim}{x}')_{Z=0} = \frac{\rho^2}{\pi^2} \iint_{Z>0} \frac{\tau(\underset{\sim}{y}) \, \tau(\underset{\sim}{z}) \, \frac{\partial^2 R_{ZZ}}{\partial R \, \partial R'}}{|\underset{\sim}{x} - \underset{\sim}{y}| \; |\underset{\sim}{x}' - \underset{\sim}{z}|} \, d\underset{\sim}{y} \, d\underset{\sim}{z} \qquad (22)$$

where the velocity covariance is

$$R_{j\ell} = \overline{u_j(\underset{\sim}{y})\, u_\ell(\underset{\sim}{z})}$$

and $\underset{\sim}{y} \equiv \underset{\sim}{y}(R, \phi, Z)$, $\underset{\sim}{z} \equiv \underset{\sim}{z}(R', \phi', Z')$.

If the turbulence is spatially locally homogeneous we can put

$$\frac{R_{ZZ}(\underset{\sim}{y}\,;\,\underset{\sim}{z})}{\sqrt{\bar{u}_Z^2(\underset{\sim}{y})}\,\sqrt{\bar{u}_Z^2(\underset{\sim}{z})}} = \bar{R}_{ZZ}(\underset{\sim}{r}) \qquad (23)$$

where $\underset{\sim}{r} = (\underset{\sim}{z} - \underset{\sim}{y})$ and $\bar{R}_{ZZ}$ is the velocity correlation coefficient. Writing $\underset{\sim}{r}(r_R, r_\phi, r_Z)$ we find that (22) becomes

$$P(\underset{\sim}{x}\,;\,\underset{\sim}{x}')_{Z=0} = \frac{-\rho^2}{\pi^2} \iint_{Z>0} \tau(\underset{\sim}{y})\,\tau(\underset{\sim}{y}+\underset{\sim}{r})\,\frac{\partial^2}{\partial r_R^2}\,\bar{R}_{ZZ}(\underset{\sim}{r}) \cdot$$

$$\sqrt{\bar{u}_Z^2(\underset{\sim}{y})}\,\sqrt{\bar{u}_Z^2(\underset{\sim}{y}+\underset{\sim}{r})}\;\frac{\cdot\, d\underset{\sim}{y}\; d\underset{\sim}{r}}{|\underset{\sim}{x}-\underset{\sim}{y}|\cdot|\underset{\sim}{x}'-\underset{\sim}{y}-\underset{\sim}{r}|} \qquad \ldots\ldots \quad (24)$$

on making the assumption that $\bar{u}_Z^2$ does not change significantly over the region in which $\bar{R}_{ZZ}$ is different from zero. In effect this is saying that $\bar{u}_Z^2$ does not vary greatly over the entire flow at a given value of R, which is not a too unreasonable assumption. If $\bar{R}_{ZZ}$ and its derivatives with respect to r_R vanish at infinity, and on the plate, an integration by parts of (24) leads to

$$P(\underset{\sim}{x}\,;\,\underset{\sim}{x}')_{Z=0} = \frac{\rho^2}{\pi^2} \int \bar{R}_{ZZ}(\underset{\sim}{r})\, d\underset{\sim}{r} \int_{Z>0} \frac{\partial}{\partial y_R}\left(\frac{\tau(\underset{\sim}{y})\,\sqrt{\bar{u}_Z^2(\underset{\sim}{y})}}{|\underset{\sim}{x}-\underset{\sim}{y}|}\right) \cdot$$

$$\cdot\; \frac{\partial}{\partial Z_R}\left(\frac{\tau(\underset{\sim}{z})\,\sqrt{\bar{u}_Z^2(\underset{\sim}{z})}}{|\underset{\sim}{x}'-\underset{\sim}{z}|}\right) d\underset{\sim}{y} \qquad (25)$$

Now it must be noted that in this analysis stationary, and not moving co-ordinates are being used. Also, as stated above $P(\underset{\sim}{x}\,;\,\underset{\sim}{x}')$, the pressure covariance on the plane $Z = 0$, is that for zero time delay and involves the instantaneous product of the fluctuating pressures at the points $\underset{\sim}{x}$ and $\underset{\sim}{x}'$ respectively. A more logical treatment would be to consider the turbulence in a frame of reference moving at some mean, or convection, speed $\bar{u}_c$. If in this frame of reference the turbulence is assumed to be isotropic, not because it is a likelihood in practice, but merely to simplify the analysis and to allow results for $P(\underset{\sim}{x}\,;\,\underset{\sim}{x}')$ to be easily computed, and to be governed therefore by the longitudinal velocity correlation coefficient $f(r';\,\tau)$, where $\underset{\sim}{r}'$ is measured relative to the moving axes, we can express $\bar{R}_{ZZ}\,(\underset{\sim}{r}\,,\,\tau)$, relative to stationary axes, in terms of $f(r_1 - \bar{u}_c\,\tau,\, r_2,\, r_3;\,\tau)$, where τ is the time delay.
$(\underset{\sim}{r}' \equiv r_1 - \bar{u}_c\,\tau,\, r_2,\, r_3)$

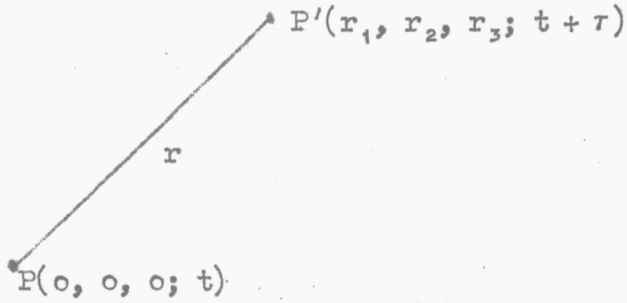

However when $\tau = 0$ we see that $f(r)$ has the same functional form as $f(r')$ and for simplicity it is this case that will, in general, be treated below. The extension to the case for general values of τ presents no difficulty in analysis but only requires pencil, paper, quiet and patience, as witnessed by the analyses in Appendices (D) and (E).

Equation (25) is the important equation in this paper. It shows that the pressure covariance at a point on the wall, due to shear flow turbulence dominated by the mean flow shear (τ), is governed by $\bar{R}_{ZZ}$, the two-point "lateral" velocity correlation coefficient, the mean shear and the turbulent intensity.

In equation (25) the integration over $\underset{\sim}{y}$ can only be effected when the values of $\tau\sqrt{\bar{u}_Z^2}$ are known. Now we can easily see that the greatest values of $\tau\sqrt{\bar{u}_Z^2}$ exist in two quite distinct regions of the wall jet at any value of the radius R. These regions are the constant stress region and the middle of the outer mixing region respectively. On the assumption that the turbulent inner region of the wall jet possesses the same structural

similarity as the inner region of a flat plate, channel or pipe flow we have that the mean velocity distribution in this region (known as the "Law of the Wall") is

$$\bar{u}/u_\tau = \frac{1}{K} \ln\left(\frac{Zu_\tau}{\nu}\right) + A \qquad (26)$$

and

$$\tau \equiv \frac{\partial \bar{u}}{\partial Z} = \frac{u_\tau}{KZ} \qquad (27)$$

where $u_\tau = \sqrt{\tau_w/\rho}$ is the shear velocity.

Equation (26) is known to hold for $\frac{Zu_\tau}{\nu} > 30$ and $Z/Z_m < 0.2$, where Z_m is the thickness of the shear layer up to the maximum velocity $\bar{u} = u_m$. K, known as the von Karman constant, has a value roughly equal to 0.4. Since the motion in this inner region must be described by universal functions of the wall shear stress, τ_w, and the viscosity, the turbulent intensity $\bar{u}_Z^2$ must be proportional to u_τ^2. From the measurements of Laufer (1955) in a circular pipe it is found that $\bar{u}_Z^2/u_\tau^2 = \alpha$ (28)

a constant over most of the inner region. (α is of the order of unity). From equations (27) and (28) we see that

$$\tau\sqrt{\bar{u}_Z^2} = \frac{\alpha}{K\nu} \frac{u_\tau^3}{\left(\frac{Zu_\tau}{\nu}\right)} \qquad (29)$$

for values of $\left(\frac{Zu_\tau}{\nu}\right) > 30$. Nearer the wall it is found that

$$\tau\sqrt{\bar{u}_Z^2} \approx 0.009 \left(\frac{Zu_\tau}{\nu}\right)^2 \frac{u_\tau^3}{\nu} \qquad (30)$$

and it is interesting to note that the maximum value of

$\tau\sqrt{\bar{u}_Z^2}$ occurs just outside the laminar sub-layer.

In fact it is very close to the region where the total turbulent intensity $\left(\bar{u}_R^2 + \bar{u}_\phi^2 + \bar{u}_Z^2\right)$ reaches its maximum value. (Fig. 1).

It is found from (29), (30) that

$$\int_0^{200} f(Z^*) \frac{dZ^*}{\left(u_\tau^3/\nu\right)^2} \simeq 0.39 \qquad (31)$$

where $f(Z^*) = \tau^2 \overline{u_Z^2}$

and $Z^* = (Z\, u_\tau/\nu)$.

On the other hand it is shown in section (8) that the value of the mean shear in the outer mixing region is

$$\tau = \frac{-0.616\, u_m}{(Z_{\frac{1}{2}} - Z_m)} \qquad (32)$$

where $Z_{\frac{1}{2}}$, Z_m are the distances to the points of half and maximum velocity respectively. On the assumption that in this latter region $\sqrt{\overline{u_Z^2}} \simeq 0.15\, u_m$ we find that

$$\tau^2 \overline{u_Z^2} = \frac{0.0085\, u_m^4}{(Z_{\frac{1}{2}} - Z_m)^2} \qquad (33)$$

This more or less completes the formal treatment of the pressure fluctuations in a wall jet. Since the contributions to $\overline{p^2}$ from the inner region and the outer mixing region are very different in magnitude (see (31) and (33)) we will consider them separately.

3. Pressure fluctuations due to the 'inner region' shear flow

From (25) we found that

$$P(\underline{x}\ ;\ \underline{x}')_{Z=0} = \frac{\rho^2}{\pi^2} \int \bar{R}_{ZZ}(\underline{r})\, d\underline{r} \int \frac{\partial}{\partial y_R}\left(\frac{\tau\sqrt{\overline{u_Z^2}}}{|\underline{x}-\underline{y}|}\right) \frac{\partial}{\partial Z_R}\left(\frac{\tau\sqrt{\overline{u_Z^2}}}{|\underline{x}'-\underline{z}|}\right) d\underline{y}$$

but in Appendix B it is shown that

$$\int \frac{\partial}{\partial y_R}\left(\frac{\tau\sqrt{\overline{u_Z^2}}}{|\underline{x}-\underline{y}|}\right) \frac{\partial}{\partial Z_R}\left(\frac{\tau\sqrt{\overline{u_Z^2}}}{|\underline{x}'-\underline{z}|}\right) d\underline{y}$$

$$= -2\pi \frac{\partial}{\partial \xi_R}\left(\frac{\xi_R - r_R}{|\underline{r}-\underline{\xi}|^2}\right) \int_o \tau^2 \overline{u_Z^2}\, dy_Z \qquad (34)$$

where $\underline{\xi} = \underline{x}' - \underline{x}$, and $\tau^2 \overline{u_Z^2}$ is assumed to be function of y_Z only.

As stated above we will assume that the turbulence is isotropic in axes moving with the convection speed $\bar{u}_c$. If the time delay is neglected

$$\bar{R}_{j\ell}(\underline{r}) = \left(f + \frac{rf'}{2}\right)\delta_{j\ell} - \frac{f'}{2r} r_j r_\ell \qquad (35)$$

where f is the longitudinal velocity correlation coefficient and $f' \equiv \frac{df}{dr}$. This form for $\bar{R}_{ZZ}$ does not agree too well with the experimental results of Grant (1958) and others. However the errors involved in the use of (35) can be shown to be small and in any case avoids the necessity for graphical or numerical integration of (25).

From (25), (34) and (35) we find that

$$P(\underline{x}\ ;\ \underline{x})_{Z=0} = \frac{2\rho^2}{\pi} \int_o \tau^2 \overline{u_Z^2}\, dy_Z \int_{r_2>0} \bar{R}_{ZZ}(\underline{r}) \left(\frac{1}{r^2} - \frac{2\, r_R^2}{r^4}\right) d\underline{r}$$

..... (36)

where $|\underline{x}| = |\underline{x}'|$, and the integration with respect to y_Z is over the whole turbulent flow giving rise to large values of $\tau^2 \overline{u_Z^2}$, and for isotropic turbulence

$$\bar{R}_{ZZ} = \left(f + \frac{rf'}{2}\right) - \frac{f'}{2r} r_Z^2 \qquad (37)$$

If the ranges of integration with respect to $\underline{r}$ are $0 < r < \infty$; $0 < \phi \leq \pi$ and $0 < \theta < \pi$

$$P(\underline{x}, 0)_{Z=0} = \frac{12\alpha}{15} \rho^2 \int_0^\infty f \, dr \int_0 \tau^2 \overline{u_Z^2} \, dy_Z \qquad (38)$$

where α is an anisotropy factor which is assumed to have a value of about $\frac{1}{3}$. If in place of (34) we use the alternative result from Appendix B (equation B.13) we find that

$$P(\underline{x}, 0)_{Z=0} = \frac{8\alpha}{15} \rho^2 < \tau^2 \overline{u_Z^2} > \int_0^\infty rf \, dr \qquad (38a)$$

where $< \tau^2 \overline{u_Z^2} >$ denotes a suitable mean value. From a comparison of (38) with (38a) it is seen that if use is made of (31)

$$< \tau^2 \overline{u_Z^2} > \approx \frac{0.6 \, u_\tau^5}{\nu \, \ell_p} .$$

If we now insert $f = \exp(-r/\ell_p)$ (39)

with $\int_0^\infty f \, dr = \ell_p$ (40)

into equation (38) we find that, with the aid of (31),

$$\frac{\sqrt{P(\underline{x}, 0)_{Z=0}}}{\frac{1}{2} \rho u_m^2} \approx 0.12 \sqrt{\left(\frac{Z_m u_\tau}{\nu}\right)} \cdot c_f \approx 5 \, c_f \qquad (41)$$

where we have used* $\ell_p = 0.14 \, Z_m$, $\frac{Z_m u_\tau}{\nu} = 1600$, and $c_f = \tau_w/(\frac{1}{2} \rho u_m^2)$ is the local skin friction coefficient. This result is similar to that found by Kraichnan (1956b) for the boundary layer on a flat plate, except our factor 5 replaces the range 2 to 12 as given by Kraichnan although we note that strictly $\sqrt{P(o)}/\frac{1}{2} \rho u_m^2$ is proportional to $c_f^{5/4}$ and $\sqrt{\frac{Z_m u_m}{\nu}}$.

---

* This value is obtained from the work of Grant (1958) by noting the zero point value of $R_{22}(r, 0, 0)$ in the region close to the wall.

Equation (41) can be compared with the results of various experimenters for ordinary boundary layer flow. The measurements of Harrison (1958) suggest a value of

$$\sqrt{\overline{p^2}} \,/\tfrac{1}{2}\,\rho\, u_m^2 \approx 0.0095 = 4.8\, c_f \qquad (42)$$

while Willmarth (1959) gives

$$\sqrt{\overline{p^2}} \,/\tfrac{1}{2}\,\rho\, u_m^2 = 0.006 = 2.5\, c_f \qquad (43)$$

Our measurement on the wall of a wind tunnel with a microphone 0.14 in. diameter and a boundary layer displacement thickness of 0.238 in. gave

$$\sqrt{\overline{p^2}} \,/\tfrac{1}{2}\,\rho\, u_m^2 = 0.008 = 3.6\, c_f \qquad (44)$$

All these results are qualitatively in fair agreement with the theory and indicate that in a turbulent boundary layer on a flat plate, in zero pressure gradient, the wall pressure fluctuation arises mainly from disturbances in the constant stress region. Since c_f changes only slowly with distance we see that $\sqrt{\overline{p^2}}$ will only change slowly with increase in x.

Finally we note that owing to the approximate nature of our analysis we are led to assume that $< \tau^2 \overline{u_Z^2} >$ is inversely proportional to ℓp with $\ell p = 0.14\, Z_m$. However the more exact analysis given in Appendix C indicates that $\tau^2 \overline{u_Z^2}$ should be averaged over a length of more nearly $0.3\, Z_m$ with ℓp given by $\ell p \approx 0.3\, Z_m$. This does not change the numerical results quoted above significantly although if anything they bring the theory more nearly in line with experiment. However the effect on the spectrum is very marked producing a two to one shift in the frequency parameter towards the lower frequencies. Further discussion on this problem is continued in Appendix E, but we conclude this section by noting that if $\ell p \approx 0.3\, Z_m$ we are not correct in assuming that the wall pressure fluctuation is dominated by disturbances in the constant stress region, but rather that the entire boundary layer, and especially the big eddies, all contribute.

4. Pressure fluctuations due to the 'outer mixing region' shear flow

In the outer region of the wall jet the structure of the turbulence is uninfluenced by the wall. Nevertheless the solution of equation (6) is still given by (19), for the contribution from the 'image' Green function must still be included. However the problem is simpler because $\tau^2 \overline{u_Z^2}$ is approximately constant over the region centred about the middle of the mixing region. Equation (25) therefore reduces to

$$P(\underline{x} ; \underline{x}')_{Z=0} = - \frac{\rho^2 \tau^2 \overline{u_Z^2}}{\pi} \frac{\partial}{\partial \xi_R} \int \bar{R}_{ZZ}(\underline{r}) \frac{(r_R - \xi_R)}{|\underline{r} - \underline{\xi}|} d\underline{r} \quad \ldots\ldots \quad (45)$$

If we again put the time lag equal to zero and put $(\underline{x}' - \underline{x}) = 0$ then

$$P(\underline{x} ; \underline{x})_{Z=0} = \frac{8\alpha}{15} \rho^2 \tau^2 \overline{u_Z^2} \int_0^\infty rf \, dr \quad (46)$$

where α is the anisotropy factor.

If further $f = \exp(-r/\ell_o)$ (47)

then

$$P(\underline{x} ; \underline{x})_{Z=0} = \frac{8\alpha}{15} \rho^2 \tau^2 \overline{u_Z^2} \ell_o^2 \quad (48)$$

On inserting the values for $\tau^2 \overline{u_Z^2}$ from (33) and putting*

$$\ell_o = (Z_{\frac{1}{2}} - Z_m) \quad (49)$$

then

$$\sqrt{\overline{p^2}}/\tfrac{1}{2}\rho u_m^2 \simeq 0.1 \quad (50)$$

The value obtained from our measurements is

$$\sqrt{\overline{p^2}}/\tfrac{1}{2}\rho u_m^2 = 0.11 \quad (51)$$

and indicates that the contribution to $\sqrt{\overline{p^2}}$ from the outer mixing region is some ten times that from the constant stress layer.

---

* This value of ℓ_o corresponds to the half-width of the outer mixing region. At first sight this value seems unduly high but it is in keeping with the results of the large eddy analysis in Appendix C and the measured spectra.

This result is not surprising when one remembers that the small shear in the outer mixing region is acting over a distance many times that of the entire inner shear layer thickness.

The theoretical value of $\sqrt{\overline{p^2}}/\frac{1}{2}\rho u_m^2$ is independent of the radius (R) and this is confirmed by our experimental results. This altogether interesting result is we feel most important for it shows that even in a region of flow, where the velocity changes in the mainstream direction are large ($u_m \sim 1/R$), the pressure fluctuations are still largely determined by local conditions only. This agrees with the results of the mean shear stress on the wall by Bradshaw and Love (1959) (Fig. 2). They showed that the skin friction coefficient, although slightly higher than for a flat plate, changed very slowly with increase in radius beyond an inner radius where the wall jet was being established.

5. The spectrum and space pressure correlation for zero time delay

In sections (3) and (4) above the formal treatment of the pressure covariance with zero time delay is given, but only the results for the mean square of the pressure are evaluated in full. However Lilley (1958) has already evaluated the pressure covariance in free shear flow turbulence, and as we have seen above the results for wall turbulence will be similar apart from a numerical factor. From Lilley's results for $P(\underline{x} ; \underline{x}')$ with $f = \exp(-\sigma^2 r^2)$, we find (Fig. 3), that $P(\underline{x} ; \xi_1, 0, 0)$ has a large negative loop with a zero crossing point of $\sigma \xi_1 \approx 1$. On the other hand $P(\underline{x} ; 0, 0, \xi_3)$ is positive for all values of ξ_3 and falls to zero as $\xi_3 \to \infty$ much slower than $f(r)$, as $r \to \infty$. The isotropic turbulence model used in evaluating these results is a little too crude to make comparison with experiment justified, apart from an order of magnitude basis, yet it is interesting to note that Harrison (1958) found similarly positive values for $P(\underline{x} ; 0, 0, \xi_3)$, although the fall off at large values of ξ_3 was slower than in our results. However this is what one might expect from the anisotropy in the large scale turbulence modifying the form of $R_{22}(\underline{r})$ at large values of $|\underline{r}|$.

The wall pressure spectrum function has been evaluated in Appendix C taking into account the large eddy structure, and in Appendix E allowing for convection. In both these cases and also in the free shear flow turbulence example the spectrum at low frequencies obeys the law $\bar{\omega}^2 \exp(-\bar{\omega}^2)$, (Fig. 4). Indeed $\overline{P}(\omega)$ must behave like ω^2 near $\omega = 0$ in an incompressible fluid. In our wall jet experiments we find such a rise at low frequencies, in contrast with all measurements made in pipes and on tunnel wall boundary layers, where the flatness of the low frequency end of the spectrum is most marked.

Harrison (1958) has also remarked on this flatness of the spectra at low frequencies and has suggested that, except at the very lowest frequencies outside the range of the measuring equipment this might be explained in terms of the intermittency of the boundary layer. However this does not in itself explain the relatively high energy content in the lower frequencies.

A complete explanation of this phenomenon has not yet been found, assuming of course that the flatness in the low frequency end of the spectra is not associated with spurious wind tunnel effects, such as fan noise, flow noise extra and above the boundary layer noise, or tunnel circuit resonance. However a clue to the explanation may come from an analysis of results similar to the space-time correlations of wall pressure obtained by Willmarth (1959)*. These data show, as explained in Appendix D, that the spatial pressure correlation for optimum time delay (i.e. roughly the autocorrelation in axes moving with the mean convection speed of the eddies) does not fall to negative values at large separation distances in contrast to the autocorrelation measured in axes fixed in the wall. This means that the life times of the big eddies are being extended on account of the growing scale associated with the slow increase in the boundary layer thickness. This consequent modification of the autocorrelation in moving axes at large times could produce the necessary lift to the low frequency end of the spectra although a fall off like $\bar{\omega}^2$ must exist at the very lowest frequencies.

On the other hand it would appear that in the case of the wall jet, since the increase in shear layer thickness is relatively large coupled with the rapid fall off in velocity with increase in radius, the life time of the eddy could not be extended in this way. These differences between the theoretical and experimental spectra for both the wall jet and boundary layer are being further investigated.

6. The wall jet - Theory of the mean flow

The wall jet has been studied theoretically by Glauert (1956) and experimentally by Bakke (1957) and Bradshaw (1959). Although Glauert found solutions for both the laminar and turbulent problems only the turbulent case will be required here. He found that the velocity distribution in the vicinity of the wall was similar to that in a boundary layer with zero pressure gradient. In the inner region one would expect the 'law of the wall' to apply but for simplicity Glauert assumed the Blasius distribution

$$\frac{\bar{u}_R^2}{u_\tau^2} = \left(\frac{\bar{u}_R Z}{\nu}\right)^{\frac{1}{4}} \Big/ \quad 0.0225 \qquad (52)$$

where u_τ is the shear velocity given by $u_\tau = \sqrt{(\tau_w/\rho)}$.

---

* Results analoguous to these have been obtained by Favre and his co-workers (1958) for the two-point velocity correlations with separation in the streamwise direction.

In the outer region Glauert evaluated the velocity distribution numerically and showed that it is slightly fuller than that given by a (1/7)th power law. The maximum velocity occurs at $Z/Z_{\frac{1}{2}} = 0.125$, for a value of $\frac{u_m}{\nu}(Z_{\frac{1}{2}} - Z_m) = 4 \times 10^4$, where $Z_{\frac{1}{2}}$ is the ordinate to the point in the outer mixing region for which $\bar{u}_R/u_m = 0.5$. The value $Z/Z_{\frac{1}{2}} = 0.125$, where $u = u_m$, differs from that obtained experimentally by Bakke, but this can be explained from Glauert's analysis, for Bakke's value of $\frac{u_m}{\nu}(Z_{\frac{1}{2}} - Z_m) = 3.5 \times 10^3$, compared with our value above of 4×10^4.

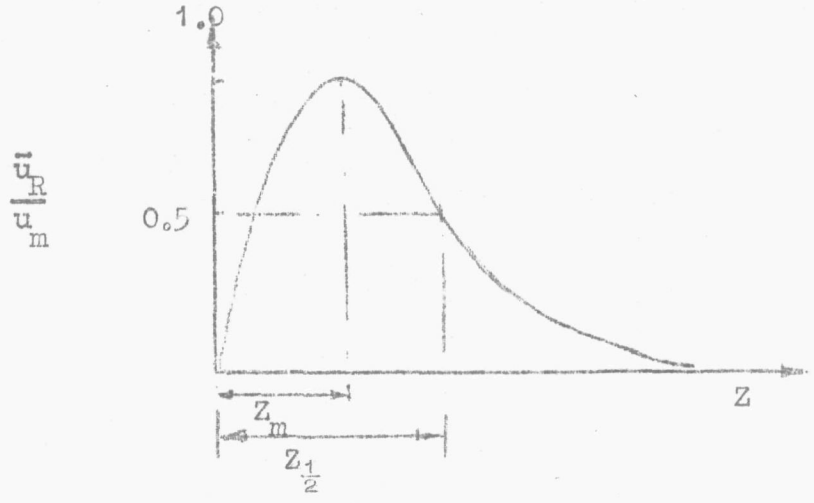

The distribution of maximum velocity with radial distance follows the law

$$\bar{u}_R \sim \frac{1}{R^{1.05}} \qquad (53)$$

at the Reynnolds numbers of the tests reported here.

The velocity distribution in the outer mixing region is found by Glauert to be given approximately by

$$\bar{u}_{R/u_m} = \operatorname{sech}^2 \left\{ 0.875 \left(\frac{Z - Z_m}{Z_{\frac{1}{2}} - Z_m} \right) \right\} \qquad (54)$$

where $Z_{\frac{1}{2}} \sim R^{0.9}$.

The experiments of Bakke confirm these predictions. Bradshaw gives some results for the variation of wall shear stress under the wall jet. These show that in the region of fully developed flow the wall shear stress is some 25% higher than in the corresponding case (i.e. equal u_m and Z_m) for the flow over a flat plate in zero pressure gradient.

7. Apparatus

Wall-Jet

The test rig shown in Fig. 5 was geometrically similar to that used by Bakke (1957) for confirmation of the theoretical results obtained by Glauert (1956). The jet was of 1.5 inch diameter and air was supplied from pressurised reservoir tanks via a 6 inch diameter throttling valve and 200 feet of 6 inch diameter pipe, part of the laboratory ring-main supply which passes horizontally 18 feet above the test site. The vertical down-pipe was of 3 inch diameter and 10 feet long connected to the 6 inch main through a 3 inch isolating valve. This was followed by a smooth contraction containing a wire gauze and then 5 feet of 1.5 inch diameter smooth-bore pipe fitted with a 6 inch diameter flange forming the jet. The jet flange was 0.75 inch above the plate.

Either of two plates were used both measuring 4 feet square. One was constructed of light acoustic boarding 2 inch thick lined with thin bakelite sheet, the other was of 2 inch thick tufnol about 100 lb in weight.

The test procedure was to open the 3 inch valve fully and to control the air-flow by the main 6 inch valve at the reservoir tanks. This was necessary to keep the valve and pipe noise to a minimum.

The measuring region was 3-10 jet diameters from the jet axis over which the jet half width (distance to half-maximum velocity) varied from 0.4 inch to 1.2 inch with maximum velocities of 140 f/s to 40 f/s.

Pressure Transducers

Ammonium di-hydrogen phosphate crystal transducers, type M213 and M141 were used. These are manufactured by the American Massa Company.

The M213 has an outside diameter 0.22 inch and a diaphragm diameter 0.14 inch. Its capacity is 12 pf and has a level frequency response to 120 kc/s. It is used with a low noise and low microphone cathode-follower connected through 6 inch of low noise cable. The input impedance of the cathode-follower is 200 megohm shunted by 6 pf, allowing a response down to 20 c/s. The cathode-follower noise level is 5 μV, although below 300 c/s the noise from the transducer is 25 μV. A high-pass filter with a cut-off at 250 c/s can be inserted, but is not normally necessary. The sensitivity at the cathode-follower in the output terminals is -111 decibels re 1 volt/microbar (approximately 2.8 microvolt/(dyne/cm^2).

The signal is amplified by a battery powered low noise amplifier of 28 decibels voltage gain, followed by an amplifier of 94 decibels voltage gain. Root mean square readings are measured on a meter of the linear averaging type. The bandwidth of the amplifiers is 5 c/s to above 500 kc/s.

The M141 has a diameter 0.6 inch, a capacity 110 pf and a sensitivity at the cathode-follower output terminals of -94 decibels re 1 volt/microbar (approximately 20 microvolts/dyne/cm^2). The low frequency noise of this transducer is much lower than the M213 due to its higher capacitance, and the usable frequency response is 20 c/s - 30 kc/s.

The transducers are mounted in the light acoustic-board plate in soft rubber sleeves and in the tufnol plate with a heavy brass body and "O" ring suspension, similar to that of Willmarth (1958). The use of the two methods of fixing in the two very different plates was to ensure that the measurements were not affected by the vibration of the transducers due to the impingement of the jet on the plate.

Spectrum measurements were made using a set of third octave filters, covering the range 40 c/s - 20 kc/s.

Turbulence Equipment

The turbulence equipment used for measurements of the fluctuating velocity in the jet was of the constant temperature kind and was a modernised version of that described by Laurence and Landes (1953), with a slightly higher bandwidth and lower noise level. Tungsten wires of 0.0002 inch diameter and 0.080 inch long were used. The hot wires were mounted on the supports using the usual copper plating technique.

Correlator

The correlator used in the space and time correlations of pressure and velocity fluctuations worked on the analogue principle. The multiplier was of the quarter-squaring type and used two special squaring valves. The design was based on that of Miller, Soltes and Scott (1955). However much improved circuitry was employed so that, if necessary, multiplication could be accomplished over the bandwidth DC - 200 kc/s. The accuracy was not of the standard associated with computing multipliers, but is of the order of 1 - 2% which is quite acceptable for the present purpose. The output was read on a DC galvanometer with a time constant variable between 2 - 10 seconds.

A time delay is accomplished on a twin channel tape recorder of extremely low wow and flutter, using one fixed and one moving head. The recorder used 0.5 inch wide tape running at 75 inch/second.

The two signals to be correlated were first recorded on a loop of tape giving a sample length of 2 seconds (this sample length could be increased if extra idling pulleys were fitted to the machine) and then

played back inserting the required time delay by manual control of the moving head. The signals could either be recorded on a frequency modulation system bandwidth DC - 20 kc/s or on an amplitude modulation system with a bandwidth of 250 c/s - 100 kc/s. The signal to noise ratio was 42 decibels.

The correlator was capable of correlating a 100 kc/s sine-wave with 15 points to the period. The maximum time delay possible was 40 millisecs and the minimum increment was 0.67 microseconds.

8. Preliminary Results and Discussion

The measurements of mean velocity across the wall jet from 3 to 10 diameters from the jet axis showed good agreement with the similarity profiles obtained theoretically by Glauert (1956) and experimentally by Baldke (1957) (Figs. 6, 7). The maximum velocity varied as $R^{-1.05}$, where R is the distance from the jet axis, and the jet half thickness $Z_{\frac{1}{2}}$ varied as $R^{0.9}$. The maximum velocity occurred at $Z/Z_{\frac{1}{2}} = 0.15$ corresponding to a Reynolds number $\frac{u_m(Z_{\frac{1}{2}} - Z_m)}{\nu} = 2 \times 10^4$.

The measurements of the wall pressure fluctuations from 3 to 10 diameters from the jet axis showed that

$$\sqrt{\overline{p^2}} / \tfrac{1}{2} \rho u_m^2 = 0.11$$

and was approximately independent of radius (Fig. 8). The corresponding spectra (Fig. 9) obeyed a similarity law on the basis of the frequency parameter $\omega(Z_{\frac{1}{2}} - Z_m) / u_m$.

Comparative results were also obtained in the College of Aeronautics 20 in. x 11 in. Low turbulence wind tunnel at a position in the working section where the displacement thickness was 0.286 in. at a freestream speed of 126 f/s. The corresponding value of the skin friction coefficient, c_f, obtained from the measured velocity profile, was 0.0022. The value of $\sqrt{\overline{p^2}}/\tfrac{1}{2}\rho u_m^2$ was 0.008 which is in fair agreement with the measurements of Willmarth and Harrison. However this result cannot be relied upon quantitatively because in this tunnel the low frequency extraneous noise level is not low, although inevitably its contribution to the total pressure energy is small. Perhaps what is more important is that it provides a check both on the accuracy of the instrumentation used, and the values of $\sqrt{\overline{p^2}}/\tfrac{1}{2} \rho u_m^2$ as found in the wall jet using the same pressure transducers.

The large values of $\sqrt{\overline{p^2}}/\frac{1}{2}\rho u_m^2$ as measured on the wall jet are not special to that case and have been found by Owen (1958) to exist on wings in regions of separated flow. However the experimental data on the effect of pressure gradient on wing pressure fluctuations is so few that we can only speculate that, on the basis of our theory, the surface pressure fluctuations will be high when either the value of c_f is high, say at transition, or the mean shear layer is very thick, say approaching and beyond separation.

9. Future Work

A more extensive study of the wall pressure fluctuations on the wall jet is in progress in which auto-correlations and space-time correlations are being made. These measurements together with two-point velocity correlation measurements will enable the equivalent eddy convection speeds to be established together with the detailed turbulent structure. It is hoped that this data, together with measurements on the effect of pressure gradient on the surface pressure fluctuations on wings, will establish the parameters on which $\sqrt{\overline{p^2}}$ must depend, and thus provide a sound basis for a better understanding of the more urgent practical problem of the nature of wall pressure fluctuations on bodies travelling at high speeds especially at supersonic and hypersonic speeds.

10. Conclusions

A review of theoretical and experimental work on wall pressure fluctuations in turbulent boundary layers is presented. The theory due to Kraichnan is modified and extended to include the separate effects of the large eddy structure and the convection of the eddies, and the treatment covers both the turbulent boundary layer on a flat plate and the wall jet. The latter case is presented for it provides data in the important practical case when the turbulence is being subjected to a rapid variation in mean shear, not unlike that associated with the flow approaching and beyond separation.

Preliminary theoretical and experimental data for the wall jet give values of $\sqrt{\overline{p^2}}/\frac{1}{2}\rho u_m^2$ many times that of corresponding measurements on a flat plate with zero pressure gradient. These results are explained in terms of the greater thickness of the shear layer, the relatively high intensity of the turbulence, and the presence of relatively large eddies in the flow.

The present work is intended as a basis for further work at both low speeds and in the more important practical areas of supersonic and hypersonic flight.

11. References

	Author		Title
1.	Bakke, P.	(1957)	An experimental investigation of a wall-jet. Jn. Fluid Mech. 2, Part 5.
2.	Batchelor, G.K.	(1951)	Pressure fluctuations in isotropic turbulence. Proc. Cam. Phil. Soc. 47, Part 2, p.359
3.	Bradshaw, P., Love, E.M.	(1959)	The normal impingement of a circular air jet on a flat surface. A.R.C. 21,268 (Sept. 1959).
4.	Curle, N.	(1955)	The influence of solid boundaries upon aerodynamic sound. Proc. Roy. Soc. A. 231 p.505
5.	Doak, P.E.	(1960)	Acoustic radiation from a turbulent fluid containing foreign bodies. Proc. Roy. Soc. A. 254, p.129
6.	Favre, A.	(1958)	Quelques resultats d'experiences sur la turbulence correlations spatio-temporelles spectres. Publications scientifiques et techniques du Ministere de l'air No. N.T.73.
7.	Feynman, R.P.	(1949)	Phys. Rev. 76, p.769
8.	Glauert, M.B.	(1956)	The wall jet. Jn. Fluid Mech. 1, Part 6, p.625
9.	Grant, H.L.	(1958)	The large eddies of turbulent motion. Jn. Fluid Mech. Vol.4 Part 2, p.149, June.
10.	Harrison, M.	(1958)	Pressure fluctuations on the wall adjacent to a turbulent boundary layer. Hydromechanics Laboratory Report 1260 David Taylor Model Basin.
11.	Heisenberg, W.	(1948)	Zur statistischen Theorie der Turbulenz. Z. Phys. 124, p.628.

References (Continued)

12.	Kraichnan, R.H.	(1956a)	Pressure field within homogeneous anisotropic turbulence. J. Acoust. Soc.Amer. 28, p.64
13.	Kraichnan, R.H.	(1956b)	Pressure fluctuations in turbulent flow over a flat plate. J. Acoust. Soc. Amer. 28, p.378
14.	Laufer, J.	(1955)	The structure of turbulence in fully developed pipe flow. NACA Report 1174
15.	Lawrence, J.C., Landes, L.G.	(1953)	Auxiliary Equipment and techniques for adapting the constant temperature hot-wire anemometer to specific airflow phenomena. NACA TN.2843
16.	Lilley, G.M.	(1958)	On the noise from air jets. ARC 20,376 Unpublished.
17.	Miller, J.A., Soltes, A.S., Scott, R.E.	(1955)	Wide-band analog function multiplier. Electronics Feb. p.160
18.	Obukhoff, A.M.	(1949)	Pressure pulsations in a turbulent flow. Ministry of Supply, England. Translation P 21452 T.
19.	Owen, T.B.	(1958)	Techniques of pressure fluctuation measurements employed in the R.A.E. low speed wind tunnels. AGARD Report 172.
20.	Phillips, O.M.	(1956)	Surface noise from a plane turbulent boundary layer. Proc. Roy. Soc. A. 234, p.327
21.	Townsend, A.A.	(1956)	The structure of turbulent shear flow. Cambridge University Press.
22.	Townsend, A.A.	(1957)	The turbulent boundary layer. Boundary Layer Research Symposium Freiburg, August 1957.
23.	Willmarth, W.W.	(1958)	Wall pressure fluctuations in a turbulent boundary layer. NACA TN. 4139.
24.	Willmarth, W.W.	(1959)	Space-time correlations and spectra of wall pressure in a turbulent boundary layer. NASA Memo 3-17-59W.

APPENDIX A

The pressure equation for the wall jet

The equations of continuity and motion for an incompressible flow are, in vector notation :

$$\nabla . (\underset{\sim}{u}) = 0 \qquad (A.1)$$

$$\frac{\rho D \underset{\sim}{u}}{Dt} = - \nabla p + \mu \nabla^2 \underset{\sim}{u} \qquad (A.2)$$

where $$\frac{D}{DT} \equiv \frac{\partial}{\partial t} + (\underset{\sim}{u} . \nabla) \qquad (A.3)$$

If in the cylindrical co-ordinate system (R, ϕ, Z) we write the corresponding velocity components (u_R, u_ϕ, u_Z), then the pressure distribution equation, found from subtracting the time derivative of (A.1) from the divergence of (A.2),

$$\nabla^2 p = - \rho \nabla . (\underset{\sim}{u} . \nabla) \underset{\sim}{u} \qquad (A.4)$$

can be written in full as

$$\begin{aligned} - \frac{\nabla p}{\rho} &= \frac{1}{R} \frac{\partial}{\partial R} R\left(u_R \frac{\partial u_R}{\partial R} + \frac{u_\phi}{R} \frac{\partial u_R}{\partial \phi} + u_Z \frac{\partial u_R}{\partial Z}\right) \\ &+ \frac{1}{R} \frac{\partial}{\partial \phi} \left(u_R \frac{\partial u_\phi}{\partial R} + \frac{u_\phi}{R} \frac{\partial u_\phi}{\partial \phi} + u_Z \frac{\partial u_\phi}{\partial Z}\right) \\ &+ \frac{\partial}{\partial Z} \left(u_R \frac{\partial u_Z}{\partial R} + \frac{u_\phi}{R} \frac{\partial u_Z}{\partial \phi} + u_Z \frac{\partial u_Z}{\partial Z}\right) \end{aligned} \qquad (A.5)$$

Now the mean velocity $\bar{\underset{\sim}{u}} = (\bar{u}_R, 0, \bar{u}_Z)$ satisfies the continuity equation

$$\frac{1}{R} \frac{\partial}{\partial R} (R \bar{u}_R) + \frac{\partial}{\partial Z} \bar{u}_Z = 0 \qquad (A.6)$$

(with Z measured normal to the plane), so that if we write R, $\bar{u}_R$ as a dimension and velocity of order unity, $O(1)$, then Z, $\bar{u}_Z$ are each $O(\delta)$ where δ is the thickness of the shear layer. Since terms involving squares and products of fluctuating quantities will be small compared with those involving products of fluctuating quantities and mean flow derivatives, the only terms of importance in (A.5) are for $R \gg 0$,

$$
\begin{aligned}
-\frac{\nabla^2 p}{\rho} &= \frac{1}{R}\frac{\partial}{\partial R}\, R\left(u_R \frac{\partial \bar{u}_R}{\partial R} + u_Z \frac{\partial \bar{u}_R}{\partial Z}\right) \\
&\quad + \frac{\partial}{\partial Z}\left(\bar{u}_R \frac{\partial u_Z}{\partial R} + u_Z \frac{\partial \bar{u}_Z}{\partial Z}\right) \\
&\doteq \frac{\partial u_R}{\partial R}\frac{\partial \bar{u}_R}{\partial R} + 2\frac{\partial u_Z}{\partial R}\frac{\partial \bar{u}_R}{\partial Z} + \frac{\partial u_Z}{\partial Z}\frac{\partial \bar{u}_Z}{\partial Z} \\
&\doteq 2\frac{\partial u_Z}{\partial R}\frac{\partial \bar{u}_R}{\partial Z}
\end{aligned}
\qquad (A.7)
$$

if mean velocity derivatives of O(1) are neglected.

APPENDIX B

The evaluation of an integral

It was shown in section 2 that the pressure correlation depends on the value of

$$I_1 = \int_{V^+} \frac{f(\underline{y}, \underline{r})\, d\underline{y}}{|\underline{x} - \underline{y}|\,|\underline{x}' - \underline{y} - \underline{r}|} \qquad (B.1)$$

where the integration is to be taken over the half-space V^+ for which $y_2 > 0$. Kraichnan (1956a) has evaluated a similar integral following the method of Feynman (1949). He found that

$$I_{\alpha\beta} = \int_V \frac{\partial}{\partial y_\alpha} |\underline{y} - \underline{x}|^{-1} \frac{\partial}{\partial r_\beta} |\underline{y} + \underline{r} - \underline{x}'|^{-1} \, d\underline{y}$$

$$= 2\pi \frac{\partial^2 |\underline{r} - \underline{\xi}|}{\partial r_\alpha \, \partial r_\beta} \qquad (B.2)$$

where $\underline{\xi} = \underline{x}' - \underline{x}$, and V the volume of integration tends to infinity.

If in (B.1) we put

$$\underline{\xi} = \underline{x}' - \underline{x}\,; \quad \underline{\eta} = \underline{y} - \underline{x}'\,; \quad \underline{\zeta} = \underline{\eta} + \underline{\xi}\,; \quad \underline{t} = \underline{\xi} - \underline{r}$$

then $$I_1 = \int \frac{f(\underline{\zeta}, \underline{r})\, d\underline{\zeta}}{\zeta\, |\underline{\zeta} - \underline{t}|} \qquad (B.3)$$

Now $f(\underline{y}, \underline{r})$ is a function which vanishes on the plane $y_2 = 0$ and at infinity. Let us suppose, for simplicity, that

$$f(\underline{y}, \underline{r}) \equiv f(\zeta_2, r_2)\,, \qquad (B.4)$$

then

$$I_1 = \int f(\zeta_2, r_2)\, d\zeta_2 \iint \frac{d\zeta_1\, d\zeta_3}{\zeta\, |\underline{\zeta} - \underline{t}|} \qquad (B.5)$$

If we introduce a new variable

$$\underline{\zeta}' = \underline{\zeta} - \frac{\underset{\sim}{t}}{1 + \tau^2} \qquad \text{with } \zeta'_2 > 0$$

(see figure below) and following Kraichnan (1956a) we use the identity

$$\frac{1}{|a| \cdot |b|} = \frac{2}{\pi} \int_0^\infty \frac{d\tau}{(a^2 + b^2 \tau^2)} \tag{B.6}$$

then

$$I_1 = \frac{2}{\pi} \int_0^\infty \frac{d\tau}{1 + \tau^2} \int_0 f(\zeta'_2, r_2)\, d\zeta'_2 \iint \frac{d\zeta'_1\, d\zeta'_3}{\left(\zeta^{12} + \frac{\tau^2 t^2}{(1+\tau^2)^2}\right)} \tag{B.7}$$

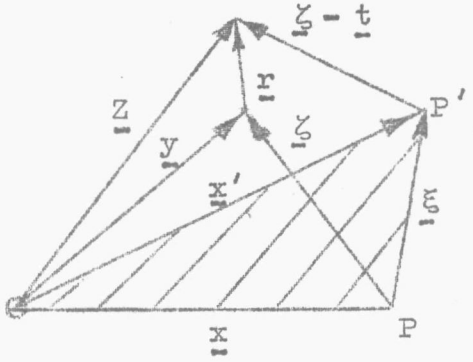

If the surface integral, with respect to ζ'_1 and ζ'_3, is taken over a circle of radius R in the plane parallel to OPP' (i.e. the wall) we find that

$$\iint \frac{d\zeta'_1\, d\zeta'_3}{\zeta^{12} + \frac{\tau^2 t^2}{(1+\tau^2)^2}} = \pi \ln \left[\frac{\zeta_2^{12} + \frac{\tau^2 t^2}{(1+\tau^2)^2} + R^2}{\zeta_2^{12} + \frac{\tau^2 t^2}{(1+\tau^2)^2}} \right] \tag{B.8}$$

Clearly we cannot continue further with the evaluation of I_1 since it tends to infinity as $R \to \infty$. However in our analysis it is not I_1 that we require, but $\frac{\partial^2}{\partial r_1^2} I_1$. If therefore we differentiate (B.7) with respect to r_1, using B.8, we find,

$$\left(\frac{\partial I_1}{\partial r_1}\right)_{R\to\infty} = 4\,t_1 \int_0 f(\zeta_2', r_2)\, d\,\zeta_2' \int_0^\infty \frac{\tau^2 d\,\tau}{(1+\tau^2)\left(t^2\tau^2 + \zeta_2'^2(1+\tau^2)^2\right)} \quad \ldots\ldots \quad (B.9)$$

In order to simplify the analysis for the pressure covariance two alternative approximations will be made in the evaluation of (B.9). In the first of these we will assume $\zeta_2'/t \ll 1$ giving

$$\frac{\partial I_1}{\partial r_1} = \frac{2\pi t_1}{t^2} \int_0 f(\zeta_2', r_2)\, d\,\zeta_2' \qquad (B.10)$$

and therefore

$$\frac{\partial^2 I_1}{\partial r_1^2} = -\frac{\partial}{\partial \xi_1}\left(\frac{\xi_1 - r_1}{|\underline{\xi} - \underline{r}|^2}\right) 2\pi \int_0 f(y_2, r_2)\, d\, y_2 \qquad (B.11)$$

In the second alternative approximation we will replace $f(\zeta_2', r_2)$ in (B.9) by a suitable mean value $\bar{f}(r_2)$. It then follows that

$$\frac{\partial I_1}{\partial r_1} = \pi \bar{f}\, \frac{t_1}{t} \qquad (B.12)$$

and

$$\frac{\partial I_1}{\partial r_1^2} = -\pi \bar{f}\, \frac{\partial}{\partial \xi_1}\left(\frac{(\xi_1 - r_1)}{|\underline{\xi} - \underline{r}|}\right) \qquad (B.13)$$

which is just half the value found in (B.2) above, for $\bar{f} = 1$, and when I_1 is taken over the whole space and not the half-space considered in our problem.

APPENDIX C

The structure of the large eddies near the wall in a turbulent boundary layer

The work of Townsend (1956), (1957) and that of Grant (1958) have shown that a relatively simple structure exists for the large eddies in a turbulent flow, or at least the experimental observations are not inconsistent with the hypothesis that the large scale motions can be adequately described in terms of relatively simple eddies. Grant's measurements of the $R_{ij}(\underline{r})$ velocity correlations at different heights from the surface in a turbulent boundary layer give rise to the suggestion that the large eddies near the surface (i.e. in the constant sress layer) have the form of 'two-dimensional' jets of fluid originating near the viscous layer, and may arise from the instability of that layer, and are roughly aligned in the direction of mean motion. Similarly in the 'outer region' the large scale turbulent motion again appears to be dominated by the presence of mixing jets of turbulent fluid which originate in the interior of the flow and penetrate to the region of the non-turbulent flow outside the boundary layer.

A simple extension of the Townsend-Grant description of the large eddy structure for such motions led us to assume that the eddies randomly distributed over all space may be described by

$$u_1 = \frac{A}{\alpha_1}(1 - \alpha_3^2 x_3^2) \exp\left(-\frac{\alpha^2 x^2}{2}\right) \qquad (C.1)$$

$$u_2 = -\frac{A}{\alpha_2}\alpha_1 x_1 (1 - \alpha_3^2 x_3^2) \exp\left(-\frac{\alpha^2 x^2}{2}\right) \qquad (C.2)$$

$$u_3 = \frac{A}{\alpha_3}\alpha_1 \alpha_3 x_1 x_3 (1 - \alpha_2 x_2) \exp\left(-\frac{\alpha^2 x^2}{2}\right) \qquad (C.3)$$

where (u_1, u_2, u_3) are the components of velocity in the directions (x_1, x_2, x_3), with x_1 in the direction of the freestream and x_2 perpendicular to the wall, and

$$\alpha^2 x^2 \equiv \alpha_1^2 x_1^2 + \alpha_2^2 x_2^2 + \alpha_3^2 x_3^2 \quad . \qquad (C.4)$$

The velocity components, given by equ. C.1 to C.3 satisfy the equation of continuity

$$\frac{\partial u_1}{\partial x_1} + \frac{\partial u_2}{\partial x_2} + \frac{\partial u_3}{\partial x_3} = 0 \qquad (C.5)$$

with $(\alpha_1, \alpha_2, \alpha_3)$ having quite arbitrary values.

Following Townsend we next find the two-point velocity correlations are given by

$$R_{11}(\underline{r}) = \frac{A^2}{\alpha_1^3\,\alpha_2\,\alpha_3} \int d\underline{\bar{y}}\,(1-\bar{y}_3^2)\left(1-(\bar{y}_3+\bar{r}_3)^2\right)\exp(-\bar{y}^2/2)\exp\left(-\frac{(\bar{y}+\bar{r})^2}{2}\right) \quad \text{(C.6)}$$

$$R_{22}(\underline{r}) = \frac{A^2}{\alpha_1\,\alpha_2^2\,\alpha_3} \int d\underline{\bar{y}}\;\bar{y}_1(\bar{y}_1+\bar{r}_1)(1-\bar{y}_3^2)\left(1-(\bar{y}_3+\bar{r}_3)^2\right)\exp(-\bar{y}^2/2) \cdot \exp\left(-\frac{(\bar{y}+\bar{r})^2}{2}\right) \quad \text{(C.7)}$$

$$\text{and } R_{33}(\underline{r}) = \frac{A^2}{\alpha_1\,\alpha_2\,\alpha_3^2} \int d\underline{\bar{y}}\;\bar{y}_1\,\bar{y}_3\,(\bar{y}_1+\bar{r}_1)\,(\bar{y}_3+\bar{r}_3)\,(1-\bar{y}_2)\,(1-\bar{y}_2-\bar{r}_2) \cdot \exp(-\bar{y}^2/2)\exp\left(-(\bar{y}+\bar{r})^2/2\right) \quad \text{(C.8)}$$

where $\bar{y}_1 = \alpha_1 y_1$; $\bar{y}_2 = \alpha_2 y_2$; $\bar{y}_3 = \alpha_3 y_3$ and $d\underline{\bar{y}} = d\bar{y}_1\,d\bar{y}_2\,d\bar{y}_3$. After integration these relations can be written in the form, if $\bar{R}_{11}$ etc. are the velocity correlation coefficients, and the subscript (b) denotes the big eddy contribution,

$$\bar{R}_{11}(\underline{r})_b = a_1\,(1-\bar{r}_3^2+\bar{r}_3^4/12)\exp(-\bar{r}^2/4) \quad \text{(C.9)}$$

$$\bar{R}_{22}(\underline{r})_b = a_2\,(1-\bar{r}_{1/2}^2)\,(1-\bar{r}_3^2+\bar{r}_3^4/12)\exp(-\bar{r}^2/4) \quad \text{(C.10)}$$

$$\bar{R}_{33}(\underline{r})_b = a_3\,(1-\bar{r}_1^2/2)\,(1-\bar{r}_3^2/2)\,(1-\bar{r}_2^2/6)\exp(-\bar{r}^2/4) \quad \text{(C.11)}$$

Grant's experimental results close to the wall suggest that

$\frac{\alpha_3}{\alpha_2} \approx 2.2$; $\frac{\alpha_3}{\alpha_1} \approx 3.0$; $\frac{\alpha_2}{\alpha_1} \approx 1.35$ whereas in the outer region

$\frac{\alpha_3}{\alpha_2} \approx 0.6$; $\frac{\alpha_3}{\alpha_1} \approx 1.5$; $\frac{\alpha_2}{\alpha_1} \approx 2.5$.

$$\text{Since} \quad R_{11}(o) = \frac{\frac{3}{4} A^2 \pi^{3/2}}{\alpha_1^3 \alpha_2 \alpha_3}$$

$$R_{22}(o) = \frac{\frac{3}{8} A^2 \pi^{3/2}}{\alpha_1 \alpha_2^3 \alpha_3} \qquad (C.12)$$

$$\text{and} \quad R_{33}(o) = \frac{\frac{3}{8} A^2 \pi^{3/2}}{\alpha_1 \alpha_2 \alpha_3^3}$$

we see that

$$\frac{\overline{u^2_2}_b}{\overline{u^2_1}_b} = \frac{\alpha_1^2}{2\alpha_2^2} \text{ and } \frac{\overline{u^2_3}_b}{\overline{u^2_1}_b} = \frac{\alpha_1^2}{\alpha_3^2} \qquad (C.13)$$

where $\overline{u^2}_{1b}$ etc. represent the big eddy contribution to $\overline{u_1^2}$ etc.
In the constant stress layer Laufer (1955) finds that

$$\overline{u_3^2}/\overline{u_1^2} = 0.5 \quad \text{and} \quad \overline{u_2^2}/\overline{u_1^2} = \frac{1}{9}$$

whilst in the outer region

$$\overline{u_3^2}/\overline{u_1^2} = 0.5 \quad \text{and} \quad \overline{u_2^2}/\overline{u_1^2} = 0.2$$

This suggests that in the constant stress region $a_2 = 2.5\, a_1$;
$a_3 = 0.9\, a_1$ whilst in the outer region $a_2 = 0.4\, a_1$; $a_3 = 0.9\, a_1$.

These results show clearly that the role of the u_2 velocity component is changed in passing from the constant stress region to the outer region.

The simple eddy structure, in the constant stress region, portrayed by these results is that of an elongated vortex ring having its longest direction in line with that of the mainstream. It is rotating in a plane parallel to the wall, whilst the longitudinal motion is wavelike, being away from and next towards the wall. The latter motion is not unlike the jet-like motion described by Townsend and thus may similarly be interpreted. In the outer region the osculations are diminished in scale whilst the eddy spreads out slightly in a direction parallel to the wall and perpendicular to the freestream.

The complete value for $\bar{R}_{22}$ must be the sum of the contributions from the small and big eddies. Thus to $\bar{R}_{22}(\underline{r})_b$ we must add on $(1 - a_2)$ times the value for $\bar{R}_{22}(\underline{r})$ obtained from the smaller eddies. If we assume that these eddies are isotropic, in contrast with the strong anisotropy of the big eddies, we have that

$$\bar{R}_{22}(\underline{r})_S = (1 - a_2) \left[f + \frac{f'}{2} \frac{r_1^2 + r_3^2}{r} \right] \qquad (C.14)$$

where $f(r)$ is the longitudinal velocity correlation coefficient and $f' \equiv \frac{df}{dr}$. Thus finally

$$\bar{R}_{22} = \bar{R}_{22(S)} + \bar{R}_{22(b)} \qquad (C.15)$$

On the assumption that

$$f(r) = \exp(-r/\ell) \qquad (C.16)$$

the values of $\bar{R}_{22}$ have been evaluated and are compared with Grant's results in Figs. 10, 11, 12 for the measurements made close to the wall (i.e. $y/\delta \approx 0.08$). Although the agreement is not good quantitatively we have qualitatively obtained results which predict the basic form of the measured results. Similar comparisons can be made for $\bar{R}_{11}$ and $\bar{R}_{33}$ both in the constant stress layer and in the outer region provided the appropriate values of a_1, a_2 and a_3 are chosen as explained above.

With these values for $\bar{R}_{22}(\underline{r})$ we can now find the two-point pressure covariance on the wall, with zero time delay. From the previous analysis we find that the pressure covariance on the wall, with the separation vector $\underline{\xi}$, is given by

$$P(\underset{\sim}{x} ; \underline{\xi} ; 0)_{\xi_2 = 0} = \frac{\rho^2}{\pi} < \tau_{12}^2 \quad \overline{u_2^2} > \int_{r_2 > 0} \bar{R}_{22}(\underline{r}) \frac{\partial}{\partial \xi_1} \frac{(\xi_1 - r_1)}{|\underline{\xi} - \underline{r}|} \cdot d\underline{r}$$

..... (C.17)

and the corresponding spectrum function is

$$\pi(\underline{x}\,;\,\kappa_1,\,0,\,\kappa_3\,;\,0) \;=\; \frac{\rho^2}{4\pi^3}\,\langle r_{12}^2\,\overline{u_2^2}\rangle \int_{r_2>0} \bar{R}_{22}\,(\underline{r})\,d\underline{r} \iint \cdot\, e^{-i(\kappa_1\xi_1+\kappa_3\xi_3)}\,\frac{\partial^2}{\partial r_1^2}\,|\underline{\xi}-\underline{r}|\;d\xi_1\,d\xi_3 \qquad (C.18)$$

Thus if $\bar{P}(\underline{x}\,;\,\kappa\,;\,0)$ is the scalar spectrum function on the surface found by averaging π over all angles in the plane, noting that

$\kappa = \sqrt{\kappa_1^2+\kappa_3^2}$ and

$$P\,(\underline{x}\,;\,0\,;\,0) \;=\; \int_0^\infty \bar{P}\,(\underline{x}\,;\,\kappa\,;\,0)\,d\kappa \qquad (C.19)$$

then

$$\bar{P}\,(\underline{x}\,;\,\kappa\,;\,0) \;=\; \frac{\rho^2}{2\pi^2}\,\langle r_{12}^2\;\overline{u_2^2}\rangle \int_0^{2\pi}\cos^2\theta\,d\theta \int_{r_2>0} d\underline{r} \cdot \left\{ e^{-\kappa r_2}(1+\kappa\,r_2)\,\bar{R}_{22}\,(\underline{r})\,e^{-i(\kappa_1 r_1+\kappa_3 r_3)} \right\} \qquad \ldots\ldots \qquad (C.20)$$

since in equation (C.18)

$$\iint e^{-i(\kappa_1\xi_1+\kappa_3\xi_3)}\,\frac{\partial^2}{\partial r_1^2}\,|\,\xi-\underline{r}|\;d\xi_1\;d\xi_3 \;=\; 2\pi\,\frac{\kappa_1^2}{\kappa^3}\,(1+\kappa r_2)\,e^{-\kappa r_2} \qquad (C.21)$$

We can now find the separate contributions to $\bar{P}$ from the small and big eddies. Thus with $R_{22(b)}$ given by equation (C.10) we find after some tedious though straightforward algebra that

$$\bar{P}\left(\underline{x}\,;\,\kappa\,;\,0\right)_b = \frac{16\,a_2\,\rho^2 < r_{12}^2\,\overline{u_2^2} > (\alpha_1/\alpha_3)^5\,(\alpha_1/\alpha_2)}{\alpha_1^3\left(1-(\alpha_1/\alpha_3)^2\right)^2}\,.$$

$$(\kappa^3/\alpha_1^3)\,\exp\left(-\kappa^2/2\alpha_1^2\right)\exp\left(-\kappa^2/2\alpha_3^2\right).\;I_2\left[\frac{\kappa^2}{2\alpha_1^2}\left(1-\alpha_1^2/\alpha_3^2\right)\right]$$

$$\left[1+\sqrt{\pi}\;\frac{e^{\kappa^2/\alpha_2^2}\,\mathrm{Erfc}\,(\kappa/\alpha_2)\,(1-2\kappa^2/\alpha_2^2)}{2\,(\kappa/\alpha_2)}\right] \qquad \ldots\ldots \qquad (C.22)$$

Similarly with $R_{22(S)}$ given by equ. (C.14) with $f(r) = \exp\left(-r^2/\ell^2\right)$ (in order to simplify the algebra but not necessarily changing the order of magnitude of the results) we find that

$$\bar{P}\left(\underline{x}\,;\kappa\,;\,0\right)_S = (1-a_2)\,\rho^2\,\ell^3\,\frac{< r_2^2\,\overline{u_2^2} >}{16}\,(\kappa\ell)^3\,e^{-(\kappa\ell)^2/4}\,.$$

$$\left[1+\sqrt{\pi}\;\frac{e^{(\kappa\ell)^2/4}\,.\,\mathrm{Erfc}\,(\frac{\kappa\ell}{2})\,(1-\frac{\kappa^2\ell^2}{2})}{(\kappa\ell)}\right]$$

A comparison between equations (C.22) and (C.23) shows that whereas the small eddy contribution to $\bar{P}$ is dominant near wave numbers of $\kappa = \ell$ (the typical energy bearing scale of the smaller class of eddies) the big eddy contribution is very dependent on the relative scales of the big eddies in the directions (x_1, x_2, x_3) respectively, i.e. $1/\alpha_1$, $1/\alpha_2$, $1/\alpha_3$.

Now in obtaining all these results it has been assumed that $R_{22}(\underline{r})$ does not change significantly with distance from the wall, which is certainly not true if, as we have shown above, we pass from the constant stress layer to the outer region. A rough comparison of equation C.22 with Willmarth's (1959) results clearly shows that since high frequency peaks beyond $\kappa\,\delta_1 = 1$ (where δ_1 is the boundary layer displacement thickness) are not present, the pressure spectrum must be determined from the form of the velocity correlation function which is not too near the wall. This means in fact that α_3/α_1 cannot be large or in other words the pressure spectrum is largely determined, up to the high frequency cut off point, from the bid eddy contributions with eddies whose transverse extent (in planes parallel with that of the wall) is not greatly different

from that in the streamwise direction. This would imply that the large eddies outside the constant stress region play a more significant role in the determination of the wall pressure fluctuations, than do the large eddies inside that region. This is not a result we might have expected from considerations of the region just outside the viscous layer in which the maximum values of the turbulent intensity and mean shear act. However it must be borne in mind that our analysis is necessarily very approximate and the reason for this result might appear more obvious if we had worked through the analysis retaining the variable mean shear and turbulent intensity instead of replacing them by an averaged value taken over the entire shear layer.

Finally in this appendix it is worth pointing out the differences which exist between our results and those of Kraichnan (1956b). Kraichnan makes the assumption that the turbulence near the wall is homogeneous in planes parallel to the wall but not in planes normal to the wall. He next assumes a model for the turbulence in which 'mirror-like' velocity boundary conditions are satisfied on both sides of the wall. In this model the u_1 and u_3 velocity components are finite on the wall but u_2 is zero. The effective correlation coefficient is then taken as

$$\tilde{R}_{22}(x_2, x_2' ; r_1, r_3) = \bar{R}_{22}(x_2 - x_2' ; r_1, r_3) - \bar{R}_{22}(x_2' + x_2 ; r_1, r_3) \qquad (C.24)$$

and when inserted into equation (C.17) it leads to the result, if $f = \exp(-\sigma^2 r^2)$,

$$\bar{P}(\underset{\sim}{x} ; \kappa ; 0) \sim \left(\frac{\kappa}{\sigma}\right)^3 \exp\left(-\left(\frac{\kappa^2}{4\sigma^2}\right)\right)\left[\sqrt{\pi}\,\frac{\left(1 + \frac{\kappa^2}{2\sigma^2}\right)\operatorname{Erfc}\left(\frac{\kappa}{2\sigma}\right) e^{\kappa^2/4\sigma^2}}{(\kappa/\sigma)} - 1\right] \qquad (C.25)$$

Numerically this result is very little different from that given by equation (C.23) but is considered less satisfactory in view of the velocity boundary conditions being essentially different from those existing in the region outside the viscous layer. Kraichnan also includes the case of variable mean shear, following the law $\tau_{12} \sim \exp(-\beta x_2)$, and although this treatment is preferable to the averaged mean shear approach which we have adopted, the results are not qualitatively different and do not lead to an order of magnitude difference in the numerical results. It would be of interest, however, to repeat our analysis with $\tau_{12} \sim \exp(-\beta x_2)$ and this is being done.

APPENDIX D

On space-time correlations of the fluctuating velocity and pressure

In the analysis above the pressure covariance has in the main been calculated for the case of zero time delay in axes fixed in the wall. However in the detailed analysis the structure of the turbulence (i.e. $R_{22}(\underline{r})$) is required in a frame moving with the turbulence and it is not immediately obvious what the relations are between the turbulence in the moving and fixed frames. This problem will now be analysed below and the results compared with the experimental results of Favre (1958) and Willmarth (1959).

Let us consider a field of homogeneous turbulence in a frame of reference moving with the mean velocity $\bar{u}_P$ past the fixed point P. In this frame of reference the four-dimensional two point velocity correlation coefficient is

$$^{(m)}\bar{R}_{ij} \quad (\underline{\Gamma}')$$

where the four dimensional vector $\underline{\Gamma}'$ between the two points in the moving frame is given by

$$\underline{\Gamma}' = (r_1' , r_2' , r_3' , r_4')$$

and r_4' is the co-ordinate representing the time delay. For example if the longitudinal velocity correlation coefficient were given by

$$f(\underline{\Gamma}') = \exp(-\alpha^2 \Gamma'^2) \quad \text{where}$$

$\alpha^2 \Gamma'^2 = \alpha_1^2 r_1'^2 + \alpha_2^2 r_2'^2 + \alpha_3^2 r_3'^2 + \alpha_4^2 r_4'^2$, then alternatively

$$f(\underline{\Gamma}') = \exp(-\sigma^2 r'^2) . \exp(-\nu^2 \tau^2) \qquad (D.1)$$

where $1/\sigma$ is a measure of the eddy length and $1/\nu$ is a measure of its life time, and

$r'^2 = r_1'^2 + r_2'^2 + r_3'^2$. This result, although not general, is typical of the connection between space and time correlations.

In a stationary frame of reference $(\underset{\sim}{r})$ in which the turbulence sweeps past at the speed $\bar{u}_p$ in the direction r_1, the relation between $\underset{\sim}{r}'$ and $\underset{\sim}{r}$ is

$$\text{with} \quad \underset{\sim}{r}' \equiv (r_1', r_2', r_3'; \tau) \text{ and } \underset{\sim}{r} \equiv (r_1, r_2, r_3),$$

$$= \left(r_1 - \int_0^\tau \bar{u}_p(\tau')d\tau', r_2, r_3; \tau\right) \tag{D.2}$$

We now make the hypothesis that the turbulence structure is unchanged in passing from fixed to moving co-ordinates. Thus with $\bar{u}_p$ independent of time, the velocity correlation coefficient in fixed axes

$$^{(f)}\bar{R}_{ij}(r_1 - \bar{u}_p\tau, r_2, r_3; \tau) = {}^{(m)}\bar{R}_{ij}(\underset{\sim}{r}') \tag{D.3}$$

Examples

(i) Zero time delay $\tau = 0$

$$^{(f)}\bar{R}_{ij}(r_1, r_2, r_3; 0) = {}^{(m)}\bar{R}_{ij}(\underset{\sim}{r}'; 0) \tag{D.4}$$

This means that the spatial correlation of velocities in a fixed frame of reference equals those in a moving frame of reference.

(ii) Zero spatial separation in fixed axes $\underset{\sim}{r} = 0$.

$$^{(f)}\bar{R}_{ij}(-\bar{u}_p\tau, 0, 0; \tau) = {}^{(m)}\bar{R}_{ij}(r_1' = -\bar{u}_p\tau, 0, 0; \tau) \tag{D.5}$$

This means that the auto correlation in a stationary frame is equivalent to a space $(r_1' = -\bar{u}_p\tau)$ and time (τ) correlation in moving axes. This is Taylor's hypothesis, which is supported by Favres' (1958) measurements in both free and shear flow turbulence.

(iii) Optimum time delay in fixed axes $r_1 = \tau_m \bar{u}_p$.

$$^{(f)}\bar{R}_{ij}(0, 0, 0; \tau_m) = {}^{(m)}\bar{R}_{ij}(0, 0, 0; \tau = \tau_m) \tag{D.6}$$

This shows that the autocorrelation using an optimum time delay in fixed axes is equivalent to finding the autocorrelation in a moving frame of reference.

These three examples are made clearer by reference to a particular velocity correlation coefficient.

Suppose that in the moving frame

$$ {}^{(m)}R_{11}\ (r_1',\ 0,\ 0;\ \tau) \ =\ \exp(-\sigma^2\ r_1'^{\,2})\ \exp(-\nu^2\ \tau^2) \qquad (D.7) $$

then in case (i)

$$ {}^{(f)}R_{11}\ (r_1,\ 0,\ 0;\ 0) \ =\ \exp(-\sigma^2\ r_1'^{\,2}) $$

$$ =\ \exp(-\sigma^2\ r_1^2) \qquad (D.8) $$

showing clearly that no change of scale occurs in changing from fixed to moving axes.

In case (ii)

$$ {}^{(f)}R_{11}\ (-\bar{u}_p\,\tau,\ 0,\ 0;\ \tau) \ =\ \exp(-\sigma^2\ \bar{u}_p^2\ \tau^2)\ \exp(-\nu^2\ \tau^2) \qquad (D.9) $$

But in the moving frame ν is of the order of $\sigma\, u'$ (where u' is the turbulent intensity) so that if $u' \ll \bar{u}_p$

$$ {}^{(f)}R_{11}\ (-\bar{u}_p\,\tau\ ,\ 0,\ 0;\ \tau) \ \approx\ \exp\ (-\sigma^2\ \bar{u}_p^2\ \tau^2) \qquad (D.10) $$

which is equal to (D.8) if

$$ r_1 \ =\ \bar{u}_p\,\tau \qquad (D.11) $$

This result is the more usual form of expressing Taylor's hypothesis.

In case (iii)

$$ {}^{(f)}R_{11}\ (0,\ 0,\ 0;\ \tau_m) = \exp(-\nu^2\ \tau_m^2) \ \approx\ \exp\ \left(-\frac{u'^2}{\bar{u}_p^2}\cdot\sigma^2\,\bar{v}_p^2\ \tau_m^2\right) $$

..... (D.12)

This shows that the autocorrelation in the moving frame can be obtained from the autocorrelation in the fixed frame (by comparing (D.10) with (D.12)) by replaing the time delay (τ) in the fixed frame by

$$\tau = \frac{u'}{\bar{u}_p} \tau_m \qquad (D.13)$$

The results of Favre (1958) for both grid and wall turbulence (Fig. 13), confirm this simple result provided that the time (τ_m) does not exceed roughly the times over which the autocorrelation in fixed axes are essentially non-zero.

Similar results might be expected to hold for the pressure covariance. Thus if we take the pressure autocorrelation in moving axes to be

$$^{(m)}P\ (0,0,0;\tau) = (1 - 2\nu^2\ \tau^2\ )\ \exp\ (-\ \nu^2\ \tau^2) \qquad (D.14)$$

then we might expect that in moving axes

$$^{(m)}P\ (r_1'\ ,\ 0,\ 0;\tau) = (1 - 2\sigma^2\ r_1'^2)\ (1 - 2\ \nu^2\tau^2)\exp(-\sigma^2\ r_1'^2)\exp(-\nu^2\tau^2) \qquad .....\quad (D.15)$$

Therefore in case (i) above

$$^{(f)}P(r_1\ ,\ 0,\ 0;\ 0) = (1 - 2\sigma^2\ r_1^{\ 2})\exp\ (-\sigma^2\ r_1^{\ 2}) \qquad (D.16)$$

In case (ii)

$$^{(f)}P(\ -\bar{u}_p\ \tau\ ,\ 0,\ 0;\tau) \approx (1 - 2\sigma^2\bar{u}_p^{\ 2})\ \exp(\ -\sigma^2\bar{u}_p^{\ 2}\ \tau^2) \qquad (D.17)$$

This result cannot strictly apply to the pressure covariance at the wall for there $\bar{u}_p = 0$. However if we assume that the turbulence is roughly convected over the plane wall at some mean speed $\bar{u}_c$* then the autocorrelation in fixed axes is found from (D.17) with $\bar{u}_p$ replaced by $\bar{u}_c$.

---

* In incompressible flow the time variation of the pressure in fixed axes, is the same as the time variation in the velocity. Thus the autocorrelation of the pressure in fixed axes, must correspond to the autocorrelation of the velocity averaged over all angles. If then the turbulence has a dominant convection speed, this speed will also apply to the pressure autocorrelation.

In case (iii)

$$(f)_P\,(0,\,0,\,0;\,\tau_m) \;=\; (1 - 2\sigma^2\,\frac{\overline{u'^2}}{\bar{u}_c^2}\,.\,\bar{u}_c^2\;\tau_m^2\;)\,.$$

$$\exp(-\,\sigma^2\,\frac{\overline{u'^2}}{\bar{u}_c^2}\;\bar{u}_c^2\;\;\tau_m^2\;) \qquad \text{(D.18)}$$

If we now consider the general case of a space-time correlation in fixed axes where $\tau \neq \tau_m$, the optimum time delay,

$$(f)_P(r_1 - \bar{u}_c\,\tau,\,0,\,0;\,\tau) = (1 - 2\sigma^2\;\;\bar{u}_c^2\;\alpha^2\;\tau^2)(1 - 2\sigma^2\,\frac{\overline{u'^2}}{\bar{u}_c^{\,2}}\;\bar{u}_c^2\;\tau^2)$$

$$.\;\exp\Big(-\;\sigma^2\;\;\bar{u}_c^2\;\;\tau^2\;\;(\alpha^2\;+\;\frac{\overline{u'^2}}{\bar{u}_c^2})\Big) \qquad \text{(D.16)}$$

$$\text{where}\quad \alpha \;=\; \Big|\;{}^{r_1}/_{\bar{u}_c\,\tau}\;\;-1\;\Big|\;.$$

According to Willmarth (1959), from measurements of the pressure fluctuations on wall turbulence we find that

$$\bar{u}_c \;\;\approx\;\; 0.8\;\;\bar{u}_1 \qquad \text{(D.17)}$$

where $\bar{u}_1$ is the freestream velocity. A comparison between Willmarth's results and those avluated from

$$(f)_P\,(r_1 - \bar{u}_c\,\tau,\,0,\,0;\,\tau) = (1 - \sigma\,|r_1 - \bar{u}_c\,\tau\,|)\;(1 - \;\nu\,|\,\tau\,|)$$

$$.\;\exp\,(-\,\sigma\,|r_1 - \bar{u}_c\,\tau\,| - \;\nu\,|\tau|) \qquad \text{(D.18)}$$

are shown in Fig. 14. The agreement is good for small time delays (i.e. up to 0.5×10^{-3} secs., which is roughly the time for non-zero autocorrelation) but is poor at large time delays.

The reason for Willmarth's results being non-negative for large time-delays probably results from the growth of the eddies as they move downstream. For small time-delays this effect is small but as the time-delay is increased the eddy-life appears to be extended as a result of this growing scale of the moving turbulence.

APPENDIX E

The evaluation of the pressure spectrum

It has been shown above that the pressure covariance at the point $\underline{x}$, with separation distance $|\underline{\xi}|$, on the wall is given by

$$P(\underline{x}\,;\,\xi_1,\,0,\,\xi_3\,;\,\tau) = \frac{\rho^2}{\pi} \quad < \tau_{12}^2 \quad \overline{u}_2^2 > \int_0^\infty dr_2 \int_{-\infty}^\infty dr_1 \int_{-\infty}^\infty dr_3 \quad \bar{R}_{22}(\underline{x};\,\underline{r};\tau) \cdot \frac{r_2^2 + (r_3 - \xi_3)^2}{|\underline{\xi} - \underline{r}|^3} \cdot \qquad (E.1)$$

If the velocity correlation coefficient is given by,

$$\bar{R}_{22}(\underline{r}';\,\tau) = e^{-\nu^2\tau^2} \quad e^{-r'^2/\ell^2}\left[1 - \frac{r_3'^2 + r_1'^2}{\ell^2}\right] \qquad (E.2)$$

where $\underline{r}'$ is the separation vector in co-ordinates moving with the turbulence. If we assume that the turbulence is convected with the constant speed u_c then in fixed co-ordinates

$$\bar{R}_{22}(\underline{r}\,;\,\tau) = e^{-\nu^2\tau^2} \quad e^{-(r_2^2 + r_3^2)/\ell^2} \quad e^{-(r_1 - u_c\tau)^2/\ell^2} \cdot \left[1 - r_3^2/\ell^2 - (r_1 - u_c\tau)^2/\ell^2\right] \qquad (E.3)$$

If we write $\bar{r}_1 = r_1/\ell$ etc and $\bar{\nu} = \frac{\nu\ell}{u_c}$; $\bar{\tau} = \frac{u_c\tau}{\ell}$

then

$$P(x\,;\,0\,;\,\tau) = \frac{4\rho^2}{\pi}\,\ell^2 < \tau_{12}^2\,\overline{u}_2^2 > e^{-\bar{\nu}^2\bar{\tau}^2} \int_0^\infty d\bar{r}_1 \int_0^\infty d\bar{r}_2 \int_0^\infty d\bar{r}_3 \left(\frac{\bar{r}_2^2 + \bar{r}_3^2}{\bar{r}^3}\right) \left[1 - \bar{r}_3^2 - (\bar{r}_1 - \bar{\tau})^2\right] \quad e^{-\bar{r}_2^2 - \bar{r}_3^2} \quad e^{-(\bar{r}_1 - \bar{\tau})^2} \cdot \qquad (E.4)$$

and the temporal spectrum function $\bar{P}(\underline{x} ; 0 ; \omega)$ is given by

$$\bar{P}(\underline{x} ; 0 ; \omega) = \frac{1}{2\pi} \int_{-\infty}^{\infty} e^{-i\omega\tau} P(\underline{x} ; 0; \tau)\, d\tau$$

$$= \frac{2 \rho^2 \ell^3 < \tau_{12}^2 \bar{u}_2^2 >}{\pi^2 u_c} \int_0^{\infty} d\bar{r}_1 \int_0^{\infty} d\bar{r}_2 \int_0^{\infty} d\bar{r}_3 \left(\frac{\bar{r}_2^2 + \bar{r}_3^2}{\bar{r}^3} \right)$$

$$\cdot e^{-(\bar{r}_2^2 + \bar{r}_3^2)} \int_{-\infty}^{\infty} e^{-i \bar{\omega} \bar{\tau}} \; e^{-\bar{v}^2 \bar{\tau}^2} \; e^{-(\bar{r}_1 - \bar{\tau})^2} \left[1 - \bar{r}_3^2 - (\bar{r}_1 - \bar{\tau})^2 \right] d\bar{\tau}$$

..... (E.5)

where $\bar{\omega} = \omega \ell / u_c$.

On taking the real part of E.5 we find that it reduces to

$$\frac{\bar{P}(\underline{x} ; 0 ; \omega)}{4 \rho^2 \ell^3 < \tau_{12}^2 \bar{u}_2^2 > / \pi^2 u_c} = \int_0^{\infty} d\bar{r}_1 \int_0^{\infty} d\bar{r}_2 \int_0^{\infty} d\bar{r}_3 \left(\frac{\bar{r}_2^2 + \bar{r}_3^2}{\bar{r}^3} \right) e^{-\bar{r}_1^2 + \bar{r}_2^2 + \bar{r}_3^2}$$

$$\cdot \int_0^{\infty} e^{-(\bar{v}^2 + 1)\bar{\tau}^2} \cos(\bar{\omega}\bar{\tau}) \left[(1 - \bar{r}_3^2 - \bar{r}_1^2 - \bar{\tau}^2) \cosh(2 \bar{r}_1 \bar{\tau}) + 2 \bar{r}_1 \bar{\tau} \sinh(2 \bar{r}_1 \bar{\tau}) \right] d\bar{\tau}$$

..... (E.6)

Now $\bar{v} \approx u'/u_c$ and is a small quantity (i.e. $\bar{v} << 1$). We can therefore neglect the term in $\bar{v}^2$ in equation E.6.

Evaluation of $\int_0^{\infty} e^{-\bar{\tau}^2} \cos \bar{\omega} \bar{\tau} \left[(1 - \bar{r}_3^2 - \bar{r}_1^2 - \bar{\tau}^2) \cosh(2 \bar{r}_1 \bar{\tau}) + 2 \bar{r}_1 \bar{\tau} \sinh(2 \bar{r}_1 \bar{\tau}) \right] d\bar{\tau} = I_1$

This integral is reduced to 3 standard integrals which can be evaluated by the use of Fourier Transforms. Thus

$$I_1 = \int_0^\infty \cos \bar{\omega}\bar{\tau}\ e^{-\bar{\tau}^2} \cosh(2\bar{r}_1\bar{\tau})\, d\bar{\tau}\,(1 - \bar{r}_3^2 - \bar{r}_1^2)$$

$$- \int_0^\infty \cos \bar{\omega}\bar{\tau}\ e^{-\bar{\tau}^2} \cosh(2\bar{r}_1\bar{\tau})\, \bar{\tau}^2\, d\bar{\tau}$$

$$+ \int_0^\infty \cos \bar{\omega}\tau\ e^{-\bar{\tau}^2} \sinh(2\bar{r}_1\bar{\tau})\, \bar{\tau}\, d\bar{\tau} \cdot 2\bar{r}_1$$

$$= \frac{\sqrt{\pi}}{2}\ e^{+\bar{r}_1^2}\ e^{-\bar{\omega}^2/4} \cos(\bar{r}_1\bar{\omega}) \left\{ \frac{1}{2} - \bar{r}_3^2 + \bar{\omega}^2/4 \right\} \qquad \ldots\ldots \quad (E.7)$$

Evaluation of $\int_0^\infty \frac{e^{-\bar{r}_1^2}}{\bar{r}^3} I_1\, d\bar{r}_1 = I_2$

From E.7 we find that

$$I_2 = \frac{\sqrt{\pi}}{2}\ e^{-\bar{\omega}^2/4} \left\{ \frac{1}{2} - \bar{r}_3^2 + \bar{\omega}^2/4 \right\} \int_0^\infty \frac{\cos(\bar{r}_1\bar{\omega})\ d\bar{r}_1}{(\bar{r}_1^2 + \bar{r}_2^2 + \bar{r}_3^2)^{3/2}}$$

$$= \frac{\sqrt{\pi}}{2}\ e^{-\bar{\omega}^2/4} \left\{ \frac{1}{2} - \bar{r}_3^2 + \bar{\omega}^2/4 \right\} \bar{\omega}\ \frac{K_1(\bar{\omega}\sqrt{\bar{r}_2^2 + \bar{r}_3^2})}{\sqrt{\bar{r}_2^2 + \bar{r}_3^2}} \qquad \ldots\ldots \quad (E.8)$$

Evaluation of $\int_0^\infty d\bar{r}_2 \int_0^\infty d\bar{r}_3\ (\bar{r}_2^2 + \bar{r}_3^2)\, e^{-(\bar{r}_2^2 + \bar{r}_3^2)}\ I_2 = I_3$

If we put $x = \sqrt{\bar{r}_2^2 + \bar{r}_3^2}$ and we use polar co-ordinates (x, ϕ) in place of $(\bar{r}_2, \bar{r}_3)$ then from E.8,

$$I_3 = \frac{\sqrt{\pi}}{2} \cdot \bar{\omega}\, e^{-\bar{\omega}^2/4} \int_0^\infty x\,dx \int_0^\pi d\phi \left\{ \frac{1}{2} + \frac{\bar{\omega}^2}{4} - x^2 \cos^2\phi \right\} \times K_1(\bar{\omega} x)\, e^{-x^2} .$$

$$= \frac{\pi^{3/2}}{2} \bar{\omega}\, e^{-\bar{\omega}^2/4} \int_0^\infty x^2 K_1(\bar{\omega} x)\, e^{-x^2} dx \,(\tfrac{1}{2} + \bar{\omega}^2/4)$$

$$- \frac{\pi^{3/2}}{4} \bar{\omega}\, e^{-\bar{\omega}^2/4} \int_0^\infty x^4 K_1(\bar{\omega} x)\, e^{-x^2} dx$$

$$= \frac{\pi^{3/2}}{8} \bar{\omega}\,(1 + \bar{\omega}^2/2)\, e^{-\bar{\omega}^2/4} \int_0^\infty \sqrt{t}\; K_1(\bar{\omega}\sqrt{t})\, e^{-t}\, dt$$

$$- \frac{\pi^{3/2}}{8} \bar{\omega}\, e^{-\bar{\omega}^2/4} \int_0^\infty t^{3/2} K_1(\bar{\omega}\sqrt{t})\, e^{-t}\, dt$$

$$= \frac{\pi^{3/2}}{32} \bar{\omega}^2 (1 + \bar{\omega}^2/2)\; \Gamma(-1, \bar{\omega}^2/4)$$

$$+ \frac{\pi^{3/2}}{32} \bar{\omega}^2 \left\{ \frac{4\, e^{-\bar{\omega}^2/4}}{\bar{\omega}^2} - 2(1 + \bar{\omega}^2/8)\; \Gamma(-1, \bar{\omega}^2/4) \right\}$$

$$= \frac{\pi^{3/2}}{8} e^{-\bar{\omega}^2/4} - \frac{\pi^{3/2}}{32} \bar{\omega}^2\, \Gamma(-1, \bar{\omega}^2/4)\,(1 - \bar{\omega}^2/4)$$

..... (E.9)

If we combine the above results then from (E.6)

$$\bar{P}(\underset{\sim}{x}\,;\,0\,;\,\omega) = \frac{\rho^2 \ell^3 \langle r_{12}^2\, \bar{u}_2^2 \rangle}{2\, \pi^{\frac{1}{2}}\, u_c} \left\{ \bar{\omega}^2/4 \cdot e^{-\bar{\omega}^2/4} - \bar{\omega}^2/4\,(1 - \bar{\omega}^2/4)\; Ei(-\bar{\omega}^2/4) \right\}$$

..... (E.10)

We note finally that

$$P(\underline{x}\,;\,0) = 2\int_0^\infty \bar{P}\,(\underline{x}\,;\,0\,;\,\omega)\,d\omega = \frac{2\,u_c}{\ell}\int_0^\infty \bar{P}\,(\underline{x}\,;\,0\,;\,\bar{\omega})\,d\bar{\omega}$$

$$= \frac{\ell^2\rho^2}{\sqrt{\pi}} < \tau_{12}^2\ \bar{u}_2^2 > \int_0^\infty d\bar{\omega}\left[\bar{\omega}^2/4\ e^{-\bar{\omega}^2/4} - \bar{\omega}^2/4\,(1-\bar{\omega}^2/4)\mathrm{Ei}(-\bar{\omega}^2/4)\right]$$

$$= \frac{8\ \ell^2\ \rho^2}{15} < \tau_{12}^2\ \bar{u}_2^2 > \qquad \ldots\ldots \qquad (E.11)$$

which is exactly double the value found by Kraichnan (1956a) for isotropic shear flow turbulence without boundaries, and provides an adequate check on the algebra leading to the spectrum function given by equation (E.10). To allow for anisotropy a multiplying factor, $\alpha \approx \frac{1}{3}$, should be inserted into E.11.

The spectrum function is plotted in Fig. 4 where the abscissa is $\frac{\omega\delta_1}{\bar{u}_1}$. δ_1 is the boundary layer displacement thickness and $\bar{u}_1$ is the freestream velocity outside the shear layer. If we take $u_c = 0.8\ \bar{u}_1$, as given by Willmarth (1959) and Harrison (1958), and $\ell/\delta_1 \doteq 2.4$ then

$$\frac{\omega\delta_1}{\bar{u}_1} = \frac{\bar{\omega}}{3} \qquad (E.12)$$

If further we insert into (E.11) the crude estimate (based on Laufer's measurements of τ_{12} and $\sqrt{\bar{u}_2^2}$ and evaluated at the value of $u_\tau\,\delta/\nu = 1550$) $\frac{\delta_1^2}{u_\infty^4} < \tau_{12}^2\ \bar{u}_2^2 > = 2 \times 10^{-5}$, and include the anisotropy factor of $\alpha = \frac{1}{3}$, then

$$\sqrt{\frac{P\,(\underline{x}\,;\,0)}{\frac{1}{4}\ \rho^2\ u_\infty^4}} = \frac{\sqrt{\bar{p}^2}}{\frac{1}{2}\,\rho\,u_\infty^2} = 9.3 \times 10^{-3},$$

compared with Willmarth's value of 0.006 and Harrison's value of 0.0095 under comparable conditions.

Similarly the peak value of $\bar{P}(\underline{x} ; 0 ; \omega)$, written in the form ,

$$\frac{2\,\bar{P}(\underline{x} ; 0 ; \omega)\,u_\infty}{\frac{1}{4}\,\rho^2\,u_\infty^4\,\delta_1} \doteq 10^{-4}$$

whereas Willmarth obtained a value of 4×10^{-5} and Harrison a value of 6.3×10^{-5}.

It should be noted that our estimates are only 3 db higher than the measured values of Willmarth and give some support to our analysis. The inclusion of the anisotropy factor is justified by Kraichnan and was similarly used by Lilley (1958) in evaluating the magnitude of the pressure fluctuations in the mixing region of a jet. Finally it might be noted that better agreement between theory and experiment might be expected, if the anisotropic form of the velocity correlation function were used, with its consequent improved scale relations to replace the ratio ℓ/δ_1 as used above.

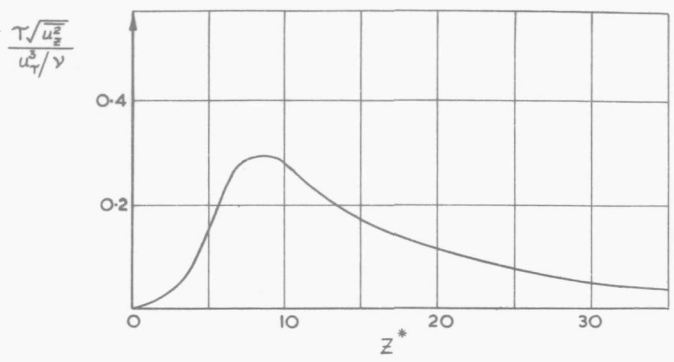

DISTRIBUTION OF THE PRODUCT OF MEAN SHEAR AND TURBULENT INTENSITY IN A BOUNDARY LAYER CLOSE TO THE WALL

FIG. 1.

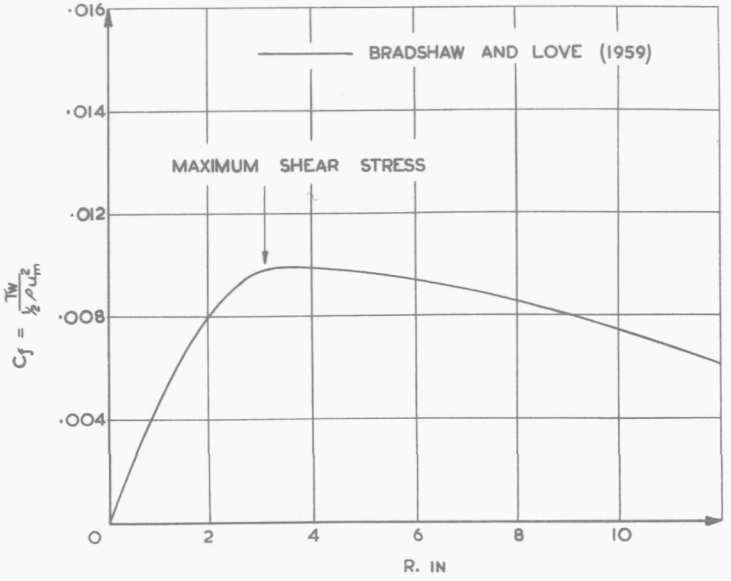

VARIATION OF THE SKIN FRICTION COEFFICIENT WITH RADIUS FOR THE WALL JET

FIG. 2.

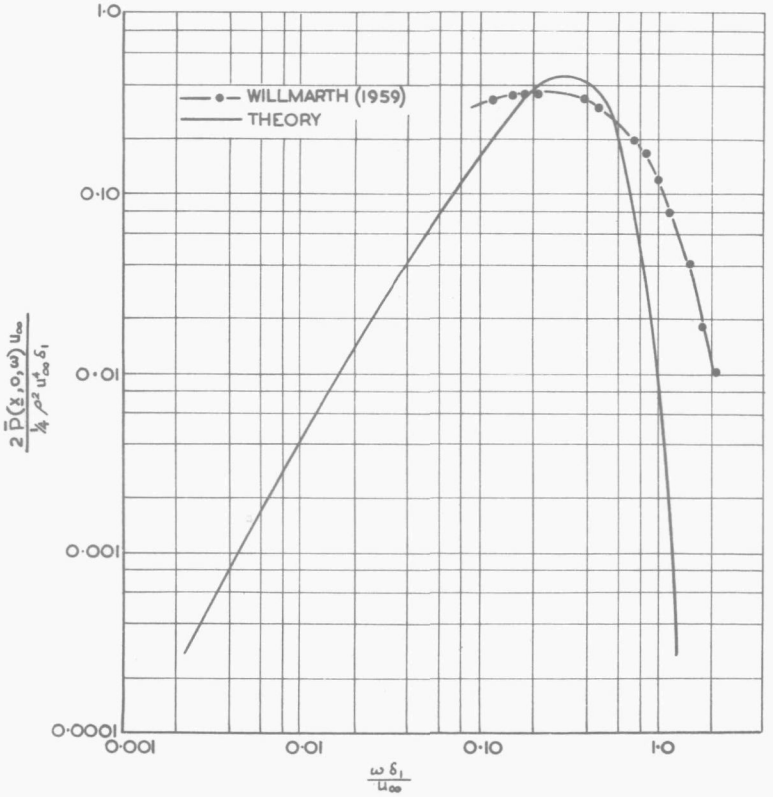

COMPARISON BETWEEN MEASURED AND THEORETICAL PRESSURE SPECTRUM FOR A BOUNDARY LAYER

FIG. 4.

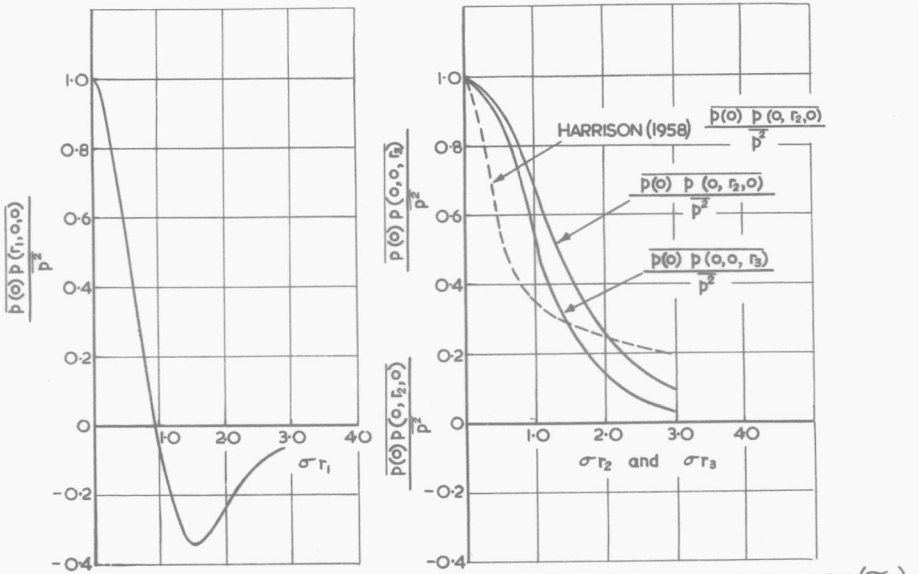

PRESSURE CORRELATIONS IN ISOTROPIC TURBULENCE SUPERPOSED ON MEAN SHEAR (T_{12})
$f(r) = \exp(-\sigma^2 r^2)$.

FIG. 3.

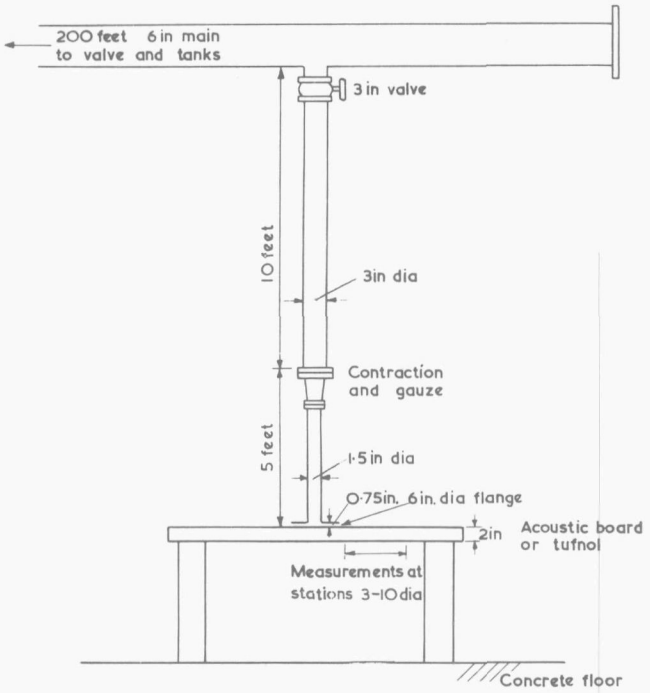

WALL JET CONFIGURATION

FIG. 5.

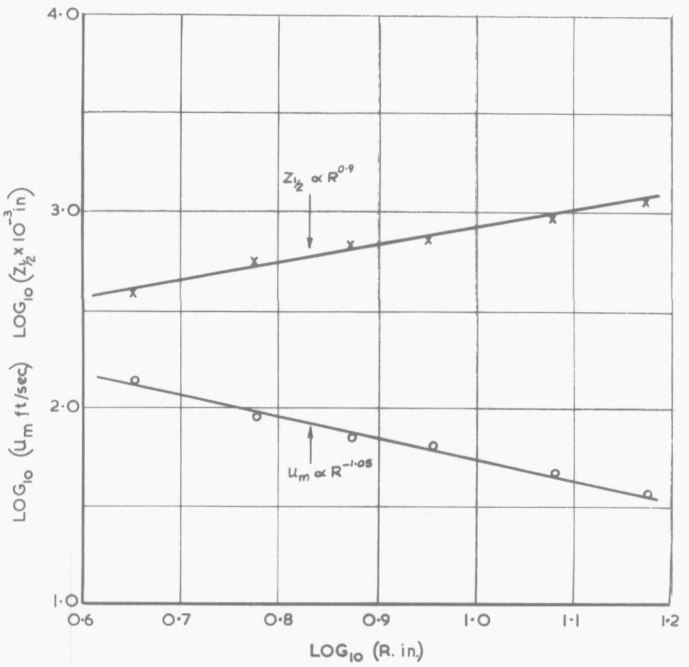

VARIATION OF WIDTH OF JET $Z_{½}$ AND MAXIMUM VELOCITY u_m WITH RADIUS R

FIG. 7.

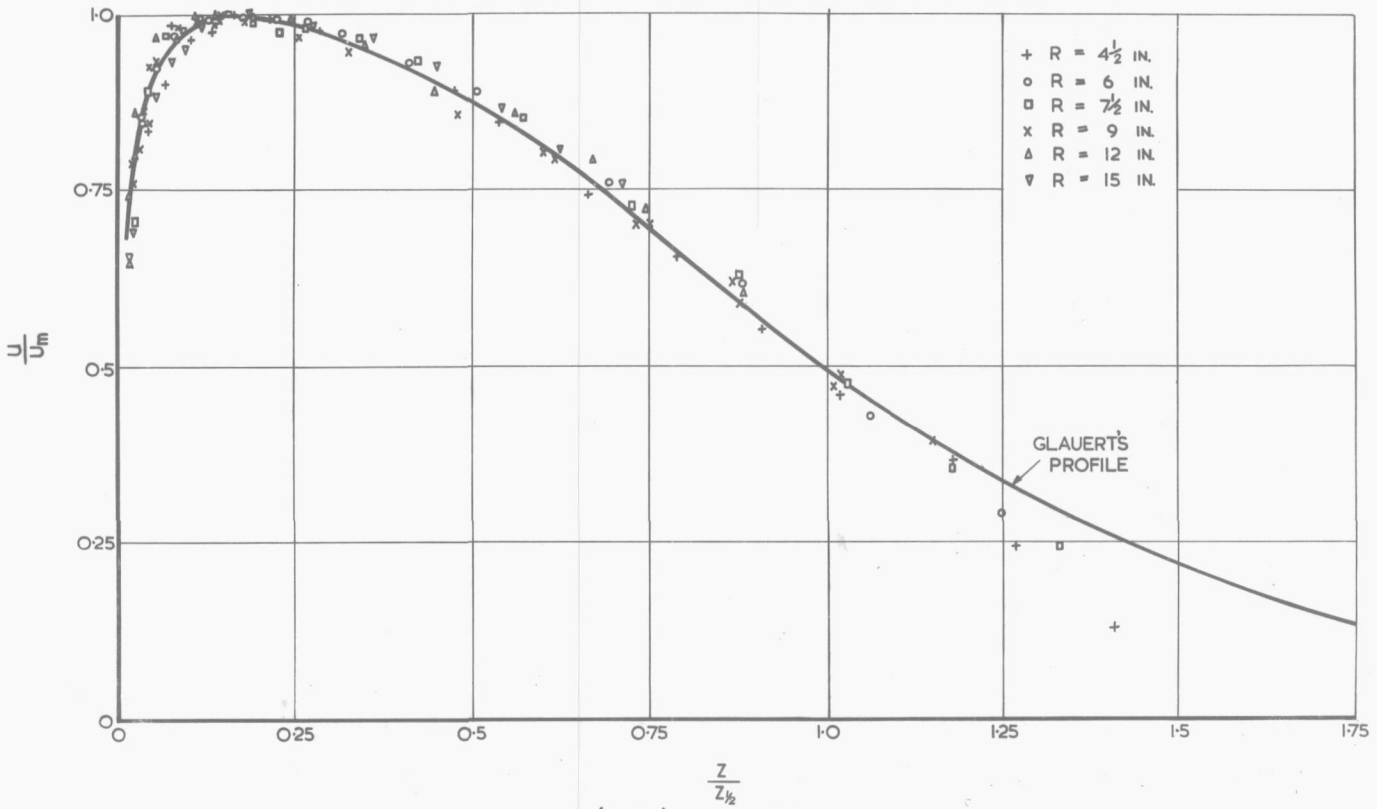

WALL JET MEAN VELOCITY PROFILES. $\frac{u_m (Z_{½} - Z_m)}{\nu} = 2 \times 10^4$, $\frac{Z_m}{Z_{½}} = 0·15$

FIG. 6.

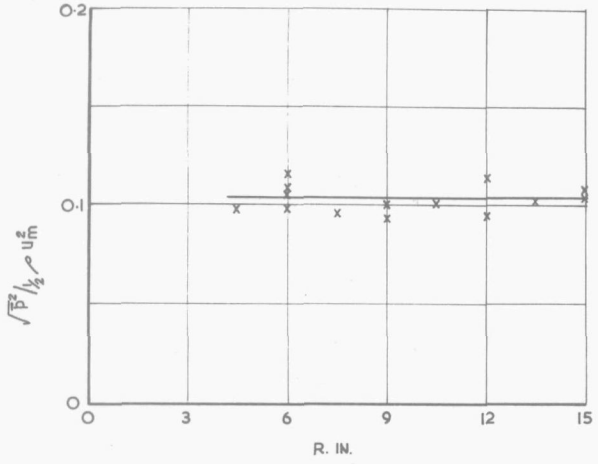

VARIATION OF $\sqrt{\overline{p^2}}/\frac{1}{2}\rho u_m^2$ WITH RADIUS R.

FIG. 8.

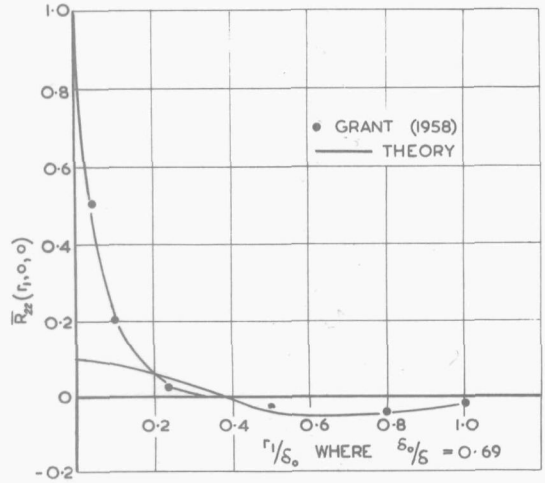

LARGE EDDY $0·1\left(1-\frac{\alpha_1^2 r_1^2}{2}\right)\exp\left(-(\alpha_1 r_1)^2/4\right)$ $\alpha_1\delta_0 = 3·73$

SMALL EDDY $0·9\left(1-r_1/2\ell\right)\exp\left(-r_1/\ell\right)$ $\frac{\ell}{\delta_0} = 0·10$

COMPARISON BETWEEN THEORY AND EXPERIMENT
FOR $\overline{R}_{22}(r_1,0,0)$ IN A TURBULENT BOUNDARY LAYER $y/\delta_0 = 0·076$

FIG. 10.

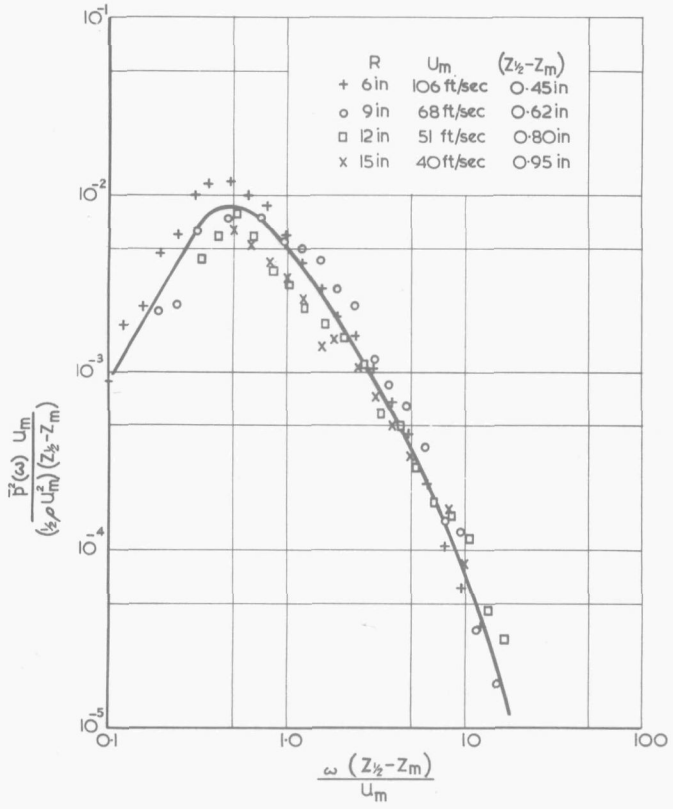

POWER SPECTRA OF WALL JET PRESSURE FLUCTUATIONS

FIG. 9.

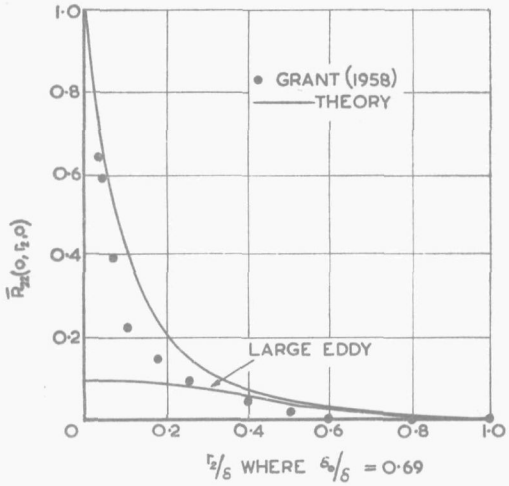

LARGE EDDY $0.1 \exp(-\alpha_2^2 r_2^2/4)$ $\alpha_1 = \alpha_2$

SMALL EDDY $0.9 \exp(-r_2/\ell)$

COMPARISON BETWEEN THEORY AND EXPERIMENT
FOR $\bar{R}_{22}(0,r_2\,0)$ IN A TURBULENT BOUNDARY LAYER $y/\delta_0 = 0.059$

FIG. 11.

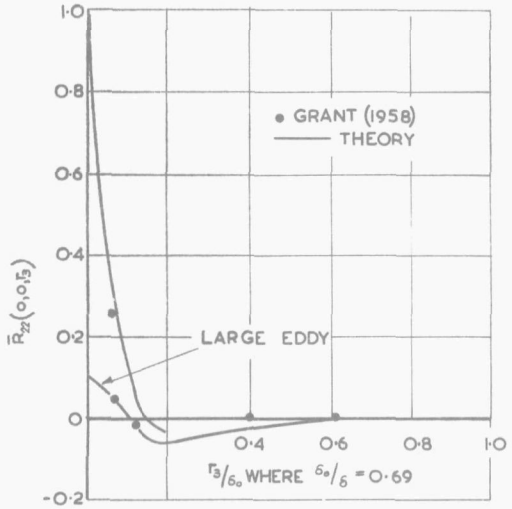

LARGE EDDY $0.1\left[1-(\alpha_3 r_3)^2+\frac{(\alpha_3 r_3)^4}{12}\right]\exp\left(-\alpha_3^2 r_3^2/4\right)$

SMALL EDDY $0.9\,(1-r_3/2\ell)\exp(-r_3/\ell)$ $\alpha_3\delta_0 = 11.1$

COMPARISON BETWEEN THEORY AND EXPERIMENT
FOR $\bar{R}_{22}(0,0,r_3)$ IN A TURBULENT BOUNDARY LAYER $y/\delta_0 = 0.052$

FIG. 12.

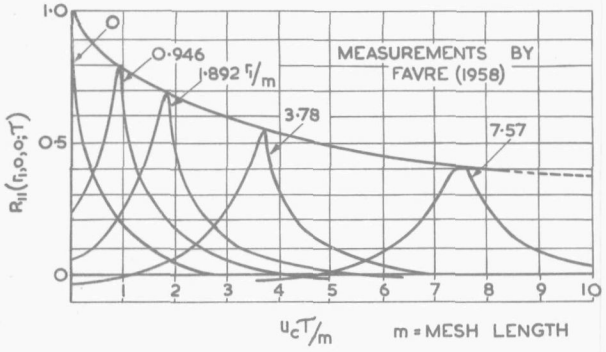

COMPARISON BETWEEN AUTOCORRELATIONS OF
$R_{11}(r_1,0,0;\tau)$ IN THE FIXED AND MOVING FRAMES
IN GRID TURBULENCE

FIG. 13.

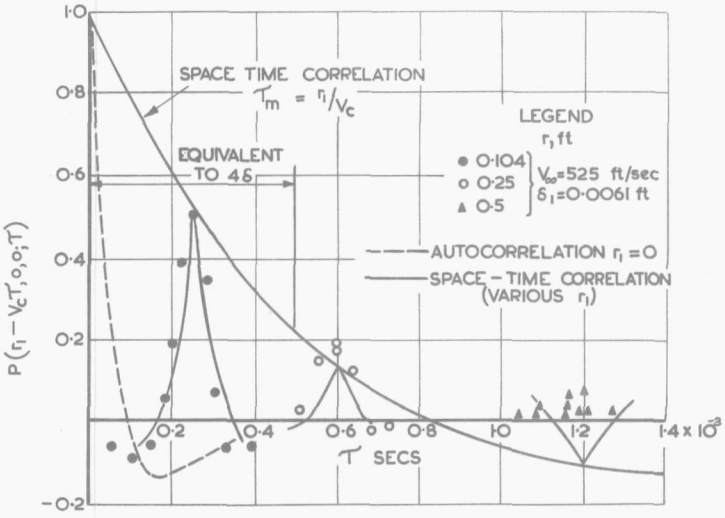

$P(r_1 - V_c\tau, r, o, o; \tau) = (1-\sigma'(r_1 - V_c\tau))(1-\nu|\tau|)\exp(-\sigma|r_1 - V_c\tau|)\exp(-\nu|\tau|)$

WITH $\nu = \sigma V'$ $\quad V_c = 0.8\,V_\infty$ $\quad 1/\sigma = 0.033$ ft $\quad V'/V_c \approx 1/10$

BOUNDARY LAYER WALL PRESSURE FLUCTUATIONS
SPACE – TIME CORRELATION
COMPARISON BETWEEN THEORY AND EXPERIMENT

FIG. 14.